THE UNIVERSITY OF ALABAMA IN HUNTSVILLE

SUMMER FACULTY FELLOWSHIP RESEARCH
CONTINUATION PROGRAM

NAG8-212
5-30165

48 P

FINAL REPORT

Submitted to:

George C. Marshall Space Flight Center
National Aeronautics and Space Administration
Marshall Space Flight Center, AL 35812

Prepared by:

Gerald R. Karr, Ph.D.
Principal Investigator
Professor and Chairman
Department of Mechanical and Aerospace Engineering
The University of Alabama in Huntsville
Huntsville, AL 35899
205/895-6154

Submitted by:

The University of Alabama in Huntsville

November 4, 1993

Abstract

This report summarizes the findings on the NASA contract #NAG8-212, Task No. 3. The overall project consists of three tasks, all of which have been successfully completed. In addition, some supporting supplemental work, not required by the contract, has been performed and is documented herein.

Task 1 involved the modification of the wall functions in the code FDNS to use a Reynolds Analogy-based method. This task was completed in August, 1992.

Task 2 involved the verification of the code against experimentally available data. The data chosen for comparison was from an experiment involving the injection of helium from a wall jet. Results obtained in completing this task also show the sensitivity of the FDNS code to unknown conditions at the injection slot. This task was completed in September, 1992.

Task 3 required the computation of the flow of hot exhaust gases through the P&W 40K subscale nozzle. Computations were performed both with and without film coolant injection. This task was completed in July, 1993.

Findings

The FDNS program tends to overpredict heat fluxes, but, with suitable modelling of backside cooling, may give reasonable wall temperature predictions.

For film cooling in the P&W 40K calorimeter subscale nozzle, the average wall temperature is reduced from 1750R to about 1050R by the film cooling. The average wall heat flux is reduced by a factor of 3.

Contents

List of Figures

Chapter 1

Introduction

1.1 Background

Analysis of film cooling in rocket nozzles by computational fluid dynamics (CFD) computer codes is desirable for two reasons. First, it allows prediction of resulting flow fields within the rocket nozzle, in particular the interaction of the coolant boundary layer with the main flow. This facilitates evaluation of potential cooling configurations with regard to total thrust, etc., before construction and testing of any prototype. Secondly, CFD simulation of film cooling allows for assessment of the effectiveness of the proposed cooling in limiting nozzle wall temperature rises. This latter objective is the focus of the current work.

A NASA code is available for the analysis of CFD processes. The FDNS (**F**inite **D**ifference **N**avier **S**tokes) code was commissioned by MSFC and was authored by SECA, Inc. in 1990. The FDNS code uses a central differencing scheme, coupled with artificial damping to capture shock waves, to solve for the heat, mass, and momentum conservation within an arbitrary geometrical domain. The code uses either a "standard" or "extended" k-ϵ turbulence model with an implementation of Launder and Spalding-like [1]wall functions for modeling of solid wall boundaries. Furthermore, the code allows for either equilibrium or finite-rate chemical reactions.

A major re-write of the code was performed over 1991-92 by Dr. Y. S. Chen, now of Engineering Sciences Incorporated (ESI). The resulting code is streamlined, has 3-D capability, but is limited to finite-rate chemical reactions. This code also has three turbulence models: standard k-ϵ, "extended" k-ϵ, and a low Reynolds number k-ϵ.

During the summer of 1991, Keith Woodbury of The University of Alabama performed computations using the NASA code FDNS for high-speed flow of air over an isothermal flat plate . The focus of his analysis was on the computed heat flux from the wall. The results showed that the FDNS code predicted heat fluxes about an order of magnitude lower than those measured under similar conditions in a shock tunnel. The explanation for the discrepancy is two-fold. First, the k-ϵ turbulence model used in FDNS does not account for the retarded velocity of the fluid in the near-wall region. Secondly, the particular form of the wall function used as a bound-

Task One.	Modify the boundary wall functions in the FDNS code to include either an implementation of either a Reynolds Analogy-based method or the Jones-Whitelaw wall function. This task addresses the code's deficiency in modeling the viscous heating near the wall.
Task Two.	Calibrate the FDNS code against published experimental data. Specifically, the code will be used to compute the helium film cooling from a wall jet.
Task Three.	Use the modified code to compute the flow of hot gases through a nozzle. For this case, the nozzle geometry currently planned for the 40K subscale nozzle test is to be used. The gas composition will be frozen, i.e., non-reacting, and the film coolant used will be ambient hydrogen.

Table 1.1: Tasks to be completed under project

ary condition for the energy equation does not adequately account for the effect of viscous heating in the near-wall region.

1.2 Project Plan

The desired objective is to use the FDNS code to predict wall heat fluxes or wall temperatures in rocket nozzles. As prior work [2] has revealed that the FDNS code is deficient in the thermal modeling of boundary conditions, the first step is to correct these deficiencies in the FDNS code. Next, these changes must be tested against available data. Finally, the code will be used to model film cooling of a particular rocket nozzle. Table 1.1 summarizes the tasks to be completed under this project.

The modifications to the FDNS code will be in the handling of the thermal boundary condition at the solid wall. The goal is to introduce as few changes as possible into the FDNS code, but enough to bring predictions from FDNS in line with available data. Previous work [2] demonstrated that a simplistic Reynolds' Analogy brought the FDNS code predictions for wall heat flux into reasonable agreement with data for the case of flow over an isothermal plate. Such a modification will be introduced in the wall functions in the FDNS code, and it will be determined if this alteration is adequate in Task 2. If not, an alternate form of the wall functions (due to Jones and Whitelaw) has been reported to yield good estimates for the wall jet problem [3] and this will be implemented and verified in Task 2.

Verification of the FDNS code modifications will be accomplished by comparing the code predictions to the experimental data of Holden [4]. The basis for comparison will be the predicted wall heat flux and the wall static pressure. Specifically, Holden's case number 45 will be considered. Case 45 is for supersonic injection of Helium coolant ($T_0 = 530\ R$, $M = 3$) parallel and into the flow of air at the nominal conditions $T_0 = 2200\ R$ and $M_\infty = 6.4$ via a wall jet.

The code will ultimately be used to compute the flow through a rocket nozzle,

with supersonic film coolant injection. The geometry of the nozzle, gas composition, and coolant injection scheme to be used in the computation will be that of the P&W 40K Subscale Nozzle. This information was disseminated at the CFD Consortium in Propulsion Technology meeting of August 1, 1991.

1.3 Supplemental Work

As a supplement to the Task 2 objective of FDNS code verification, the code will be used to compute the flow of hot exhaust gases through a 40K combustor. This combustor is the same as the configuration tested by Dexter [5] at MSFC. This article was fitted with a calorimeter jacket, and the data from Dexter was obtained for comparison. This provides a measure of the suitability of the code for use in combusting, accelerating flows.

As a supplement of Task 3, a novel approach to solution of the conjugate heat transfer problem will be used. This approach provides a simple, iterative method which can be applied when adequate knowledge of the backside cooling is available.

Chapter 2

Task 1: Wall Functions

Task 1 of the project was completed in August, 1992. The then-current version of the code was obtained from Dr. Y. S. Chen of ESI on August 3, 1992. This version contained a heat flux wall function similar to the one recommended by Woodbury [2]. This function was modified to make it conform to the Reynolds-Analogy desired for this project.

The current formulation of the code, the wall function for the energy equation has a form

$$q_w = (h_w - h_p - \mathrm{Pr}_t(u_p - u_w)^2/2)(\tau_w/u_p) \tag{2.1}$$

where h_w and h_p are the enthalpies of the wall and the adjacent point away from the wall, respectively; u_w and u_p are the velocities, τ_w is the wall shear stress, and Pr_t is the turbulent Prandtl number, taken to be $\mathrm{Pr}_t = 0.90$.

Note that this wall function is similar to the Reynold's Analogy model proposed in Reference [2]. That function follows from the definition of the heat transfer coefficient, h_{conv} for a compressible boundary layer (Shapiro [6], page 1100)

$$q_w = h_{conv}(T_{aw} - T_w)$$

where T_{aw} is the *adiabatic wall temperature*, and T_w is the actual wall temperature. If the adiabatic wall temperature (given by Shapiro [6], page 1099) is

$$T_{aw} = T_\infty + RU_\infty^2/2/c_p$$

which defines the *recovery factor*, R. ($R \approx 0.89$ for air.) Then, with the *Reynolds Analogy* (as suggested by Shapiro ([6], page 1100), and verified experimentally by Holden ([7], Figure 12a), expressed as

$$\frac{C_f}{2} = \frac{\tau_w}{\rho U_\infty^2} \approx C_H = \frac{h_{conv}}{c_p \rho U_\infty}.$$

the heat transfer may be inferred based on the wall friction as

$$q_w = \frac{\tau_w c_p}{U_\infty}(T_\infty - T_w) + \frac{\tau_w}{2} U_\infty R.$$

Or,

$$q_w = \frac{\tau_w}{U_\infty}(h_\infty + R\frac{U_\infty^2}{2} - h_w) \tag{2.2}$$

where h is the *enthalpy*, **not** the heat transfer coefficient. Comparing Equation 2.1 with Equation 2.2, and recognizing that Pr_t is numerically equal to R, it can be seen that the expressions are substantially the same.

The wall functions are implemented using a dimensionless distance y^+. This distance is defined in terms of the resulting shear stress at the wall as $y^+ = y\sqrt{\tau_w/\rho}/\nu$. The wall functions implemented in this version are claimed to be accurate over a range of $60 < y^+ < 700$.

Chapter 3

Task 2: Verification

3.1 Background

Task 2 was completed in September, 1992. This task involved using the FDNS code to predict the heat flux from a $M = 3$ Helium wall jet. The actual case is documented in the experimental work of Holden [4].

In Holden's report, specific information about the actual profile conditions (velocity and temperature) at the jet injection point were not available. This led to a parametric study in the present investigation to determine the effects of various assumptions about these conditions.

This effort is made to study the effects of inlet boundary conditions of the injection on the wall heat transfer downstream of the injection slot. Results that follow are all for test condition "Run 45" one of the test cases in Holden's report[4]. Computations are carried out for a grid containing 121 by 41 mesh points. Grid spacing has been adjusted to ensure convergent solutions and desired dimensionless normal distance y^+ within the range of $60 < y^+ < 700$, as is suggested by the author of the code, Dr. Y. S. Chen.

In all cases, turbulence quantities k and ϵ are assumed to be uniform at the exit of the injection slot, and are given by

$$k = 0.001 U_{ref}^2 = \text{Constant}$$

$$\epsilon = \frac{C_\mu (k)^{3/2}}{0.03 X_{ref}} = \text{Constant}$$

3.2 Inlet Profile Effects

Fig. 3.1 shows the effects of the inlet temperature profile on the heat transfer downstream of the slot. In the figure, Holden's data are compared to computed results from FDNS for both a constant inlet temperature and a turbulent inlet temperature profile. In the computed results, the velocity profile at the inlet was taken as uniform. The turbulent inlet temperature profile was obtained from a contour map of computed results for analysis of the injection nozzle alone. These injection nozzle

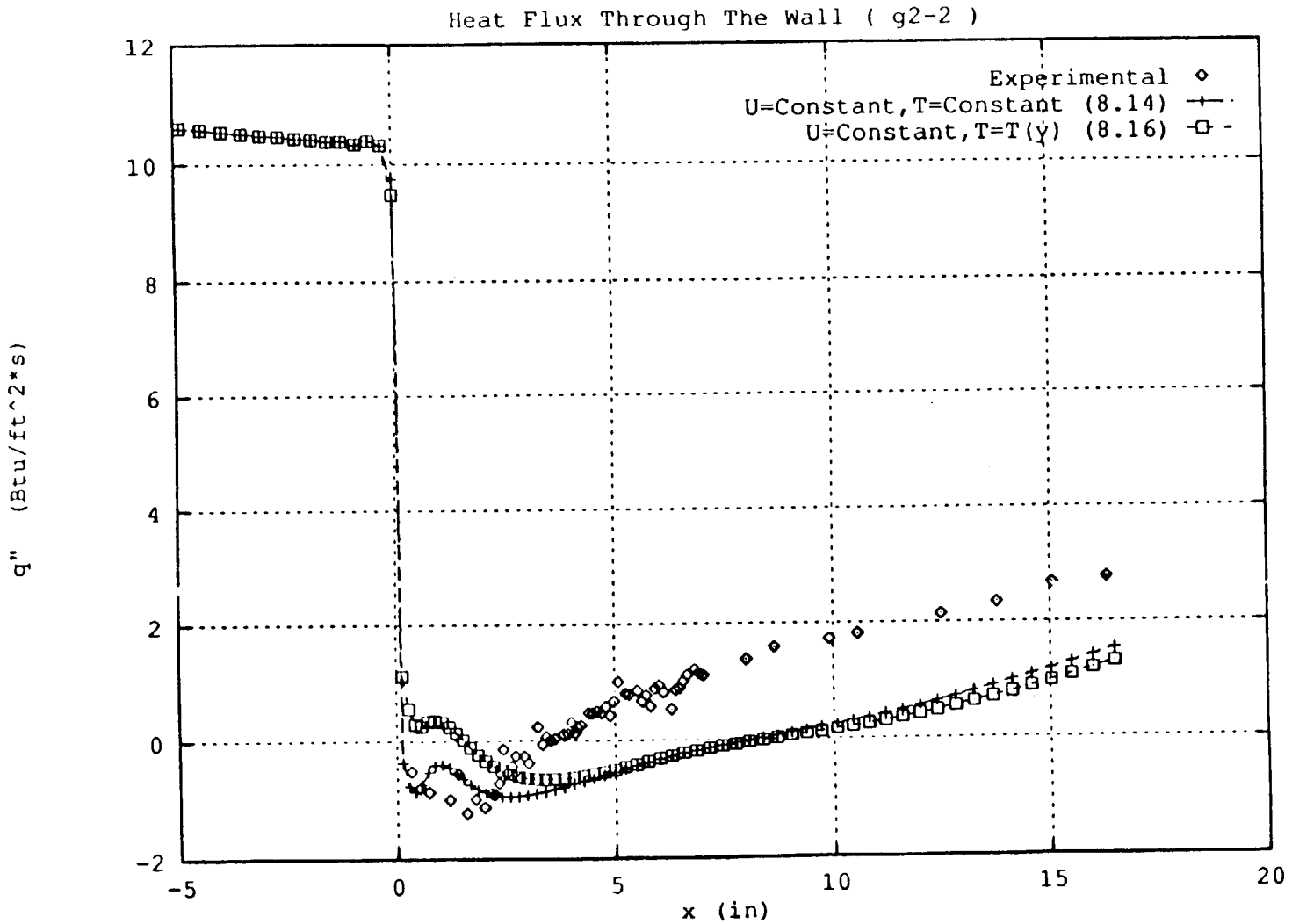

Figure 3.1: Effect of Turbulent Inlet Temperature Velocity Profile

computations were performed by Dr. Y. S. Chen[8]. This profile was approximated by curve fit as

$$T(y) = 0.321 T_{ref} \left[\frac{y}{h/2}\right]^{-0.3831}$$

This figure shows that the effect of temperature profile on the predicted wall heat flux is limited to a distance of 2 inches (about 30 – 35 times the slot height) from the slot. In this region, Chen's profile predicts a higher heat flux than the experimental result.

Fig. 3.2 incorporates Chen's results for temperature and velocity at the injection nozzle. The result, denoted 8.28 in the figure, underpredicts the heat flux over most of the flow region.

Fig. 3.3 show the effect of the laminar versus turbulent velocity profiles on the downstream wall heat flux. For these calculations, the inlet temperature profile was assumed uniform. In the figure, the results corresponding to the turbulent velocity profile are denoted as 8.18, and those for the laminar assumption as 8.25. The turbulent profile again was assumed as the 1/7 power law, and a simple parabolic assumption was made for the laminar profile:

$$U(y) = \frac{3}{2}(4967.77)\left[\frac{y}{h/2}\right]^{2}$$

The laminar profile results in a very strong decrease, then an increase, in heat flux over a short distance. This confirms that the assumption of a laminar velocity profile at the slot inlet is clearly unreasonable.

Fig. 3.4 shows the effect of varying the inlet velocity profile. In this figure, both computations use Chen's temperature profile, but one (denoted 8.16) uses uniform velocity profile, while the other (denoted 8.18) uses an approximate turbulent profile (the 1/7 power law):

$$U(y) = 4967.77\left[\frac{y}{h/2}\right]^{1/7}$$

It can be seen from this figure that the turbulent velocity profile does not result in a better prediction than the uniform one.

3.3 Additional Verification

3.3.1 40K Combustor Data

Further measures were taken to test the usefulness of the FDNS code for determination of wall heat fluxes in the presence of a combusting, accelerating flow. A 40K calorimeter combustor, manufactured by Pratt and Whitney, had been hot-fired at MSFC and data from one of these firings was used to test the computer code. A second benefit of this exercise is to determine the conditions of the hot gas which will be entering the subscale nozzle.

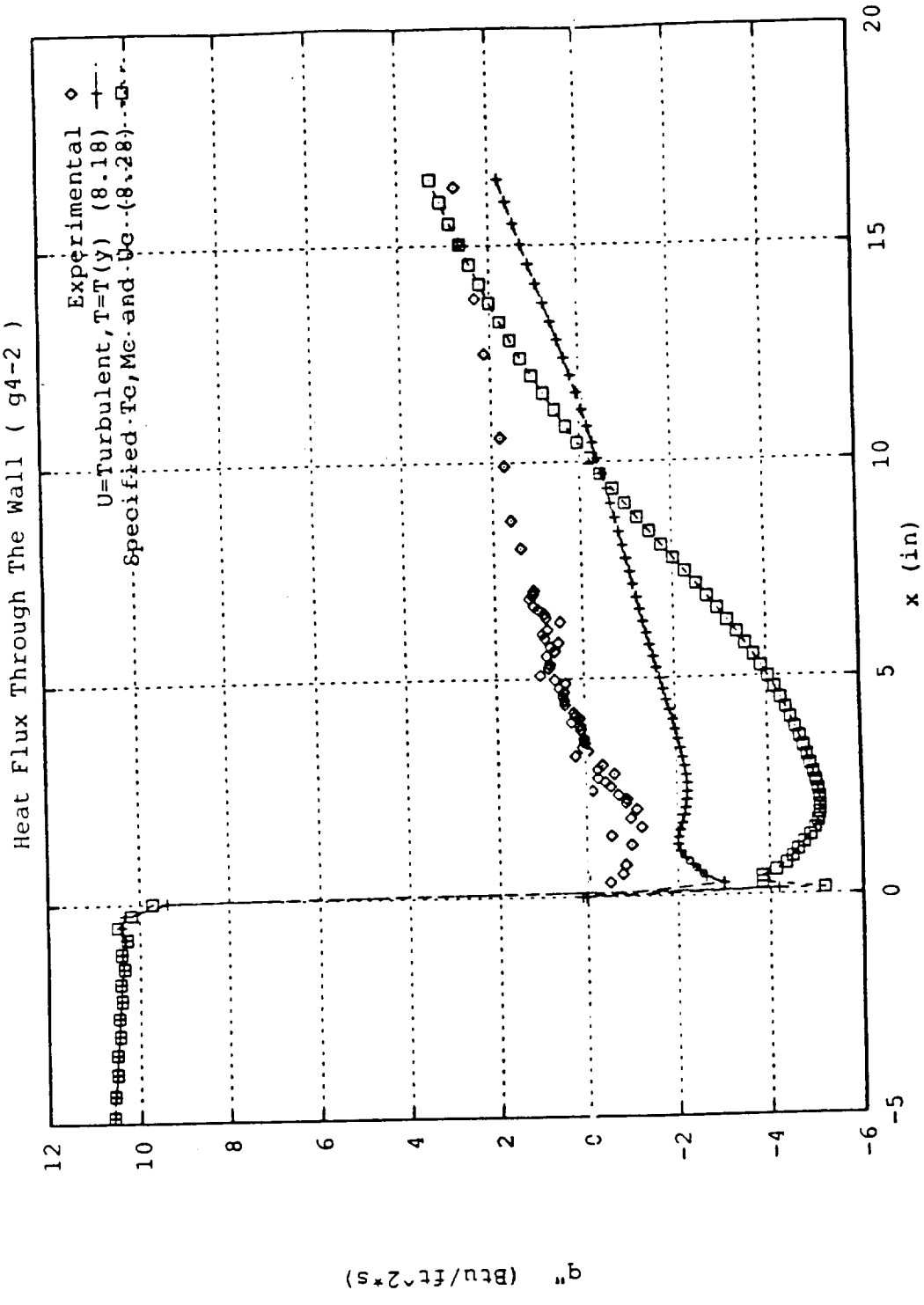

Figure 3.2: Effect of Computed Inlet Temperature and Velocity Profiles

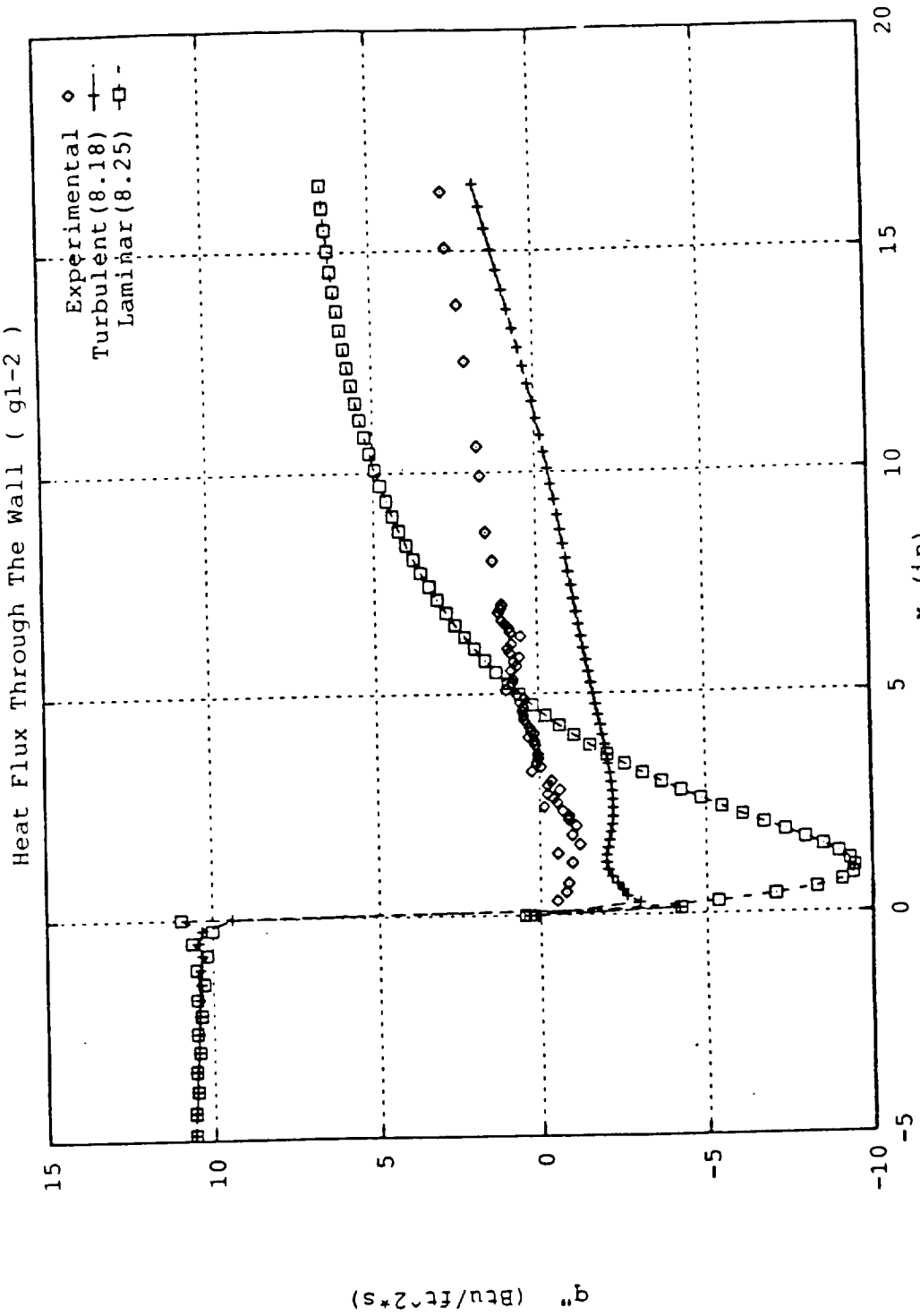

Figure 3.3: Laminar versus Turbulent Velocity Profile Effects

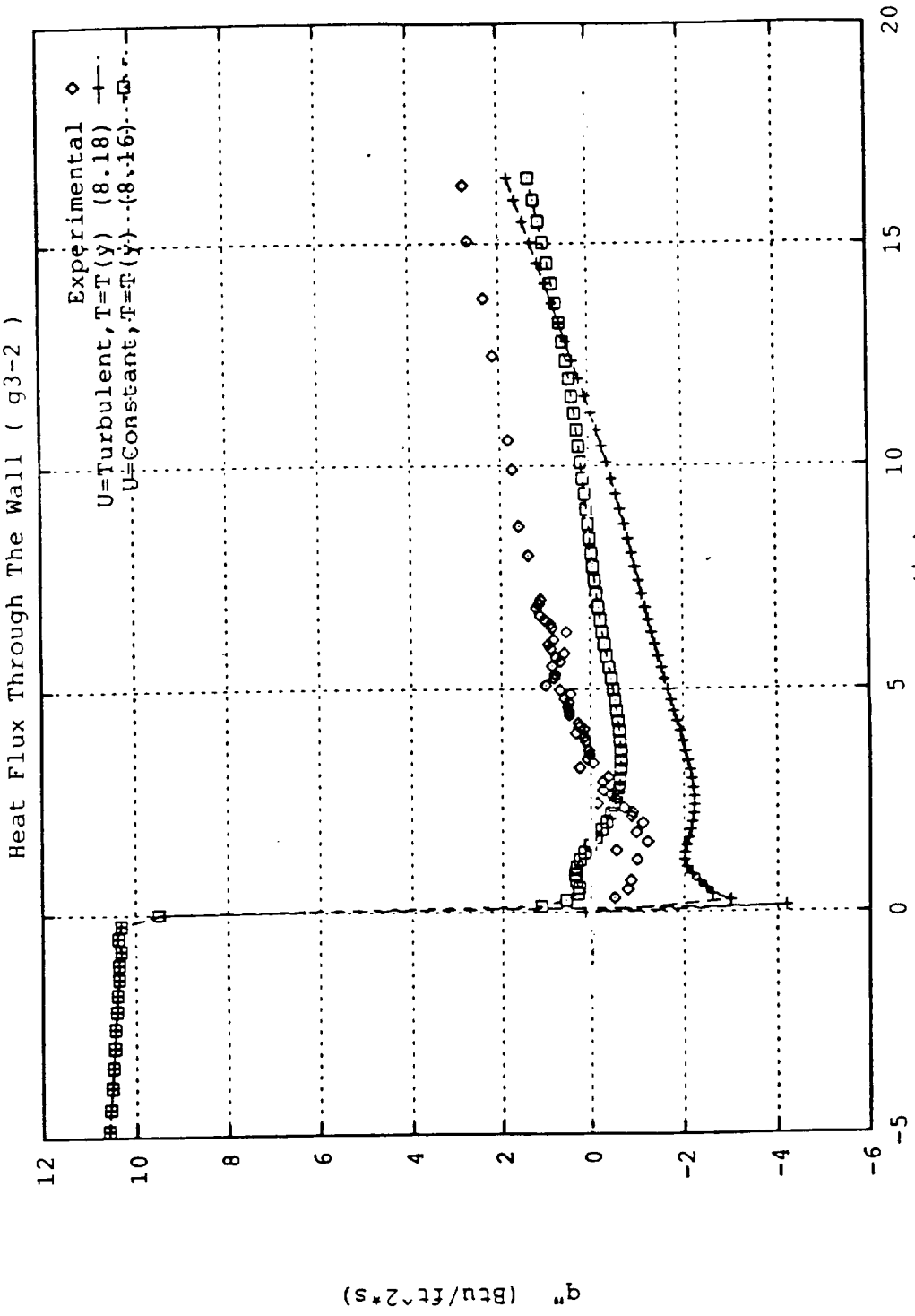

Figure 3.4: Effect of Turbulent Inlet Velocity Profile

O/F	6.00	7.5	4.0
P_c (PSIA)	1775	1750	1750
T (R)	6422	6629	5392
ρ (slug/ft^3)	0.01055	0.01164	0.00918
γ	1.1442	1.1336	1.1929
Mach No.	0.203	0.203	0.203
U (ft/sec)	1055.8	993.4	1147.3
H_2O (α_1)	0.6723	0.7213	0.4970
O_2 (α_2)	0.0032	0.0223	0.0000
H_2 (α_3)	0.2483	0.1327	0.4894
O (α_4)	0.0030	0.0105	0:0000
H (α_5)	0.0313	0.0294	0.0100
OH (α_6)	0.0418	0.0835	0.0035

Table 3.1: ODE Results for Three O/F Ratios

A test case was chosen from many available by consultation with Carol Dexter of MSFC [5]. The case, Run 027, had an O/F ratio of exactly 6.00, and the data supplied by Dexter is included in the appendix.

The FDNS program requires the composition, velocity, and turbulence level of the hot gas at the head end of the combustor, as well as the distribution of temperature along the combustor wall. Here the complex details of the mixing and combustion of the fuel and oxidizer are ignored; it is assumed that the hot gaseous products of combustion enter the chamber with their initial velocity. The ODE program was used to obtain the inlet conditions including gas composition, pressure, temperature, and velocity. Table 3.1 gives the ODE results for O/F ratios of 6.00, 7.5, and 4.0. The first column was used to provide the required inlet information.

The experimentally measured temperatures along the hot combustor wall were used to specify the wall conditions. Although this is not *predictive*, since the wall temperatures are being specified based on an experiment, it was considered to be the best test of the ability of the FDNS code to determine the wall heat flux. That is, if the exact wall temperature distribution is supplied, then any differences observed between the computed and actual (measured) wall heat flux will not be due to uncertainties in the wall temperatures. A spline routine was used to interpolate the data supplied by Dexter to determine the appropriate wall temperature for each computational node along the wall.

The unknown turbulence parameters (k, ϵ) of the hot gases entering the combustor was problematic. An incremental approach was adopted: beginning with low levels of kinetic energy k, successive solutions were obtained with FDNS and the heat flux results compared to the data from Dexter. It was found that higher values of k gave the best results; however, convergent solutions could not be obtained for $k > 0.1U^2$. Hence, the level of turbulence at the inlet of the combustor was fixed at $k = 0.1U^2$.

The results of the FDNS computation are shown in Figure 3.5. As can be seen, the FDNS results are double those obtained by calorimetry. *Note, however, that the*

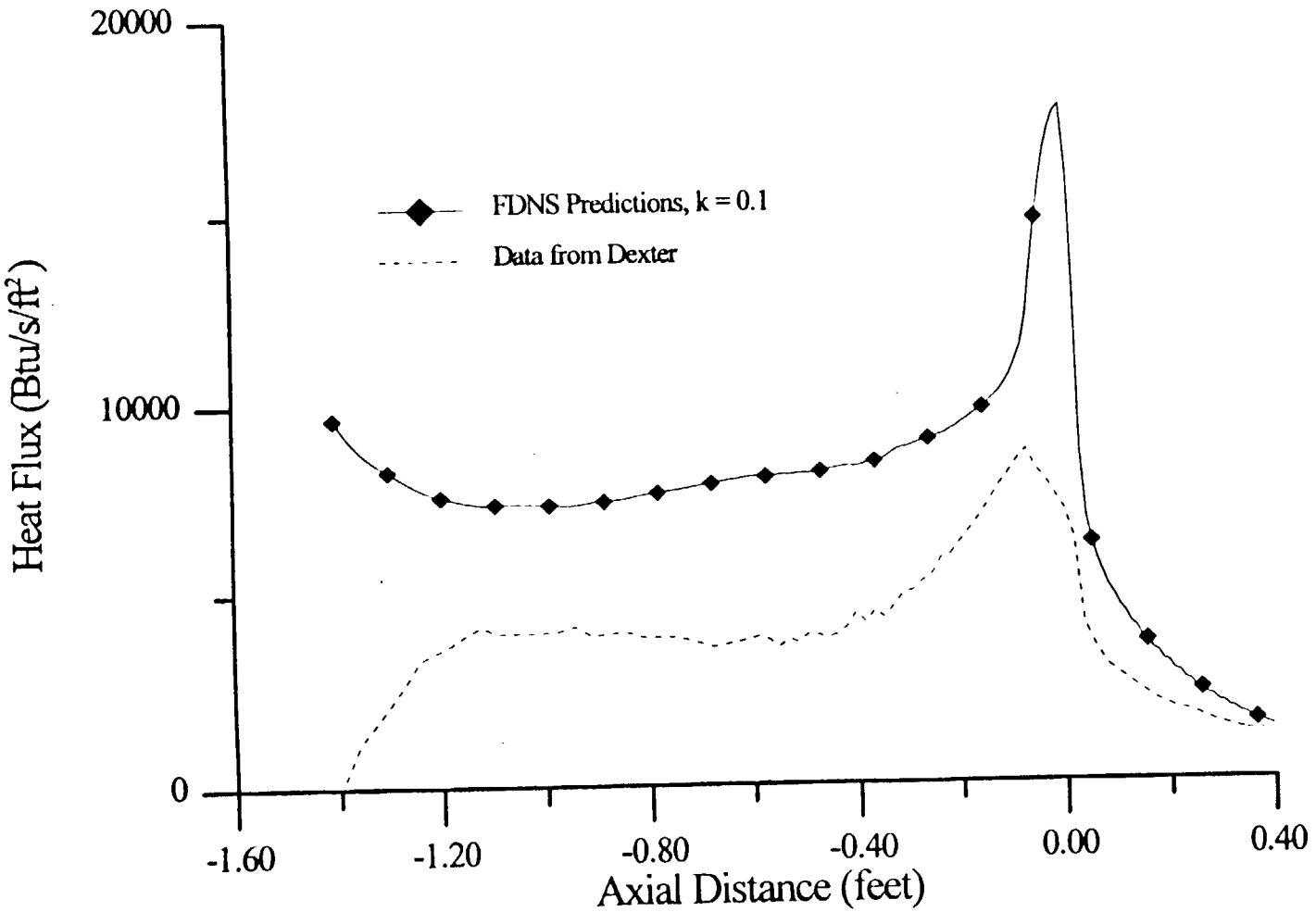

Figure 3.5: Comparison of FDNS Wall Fluxes with Data for 40K Chamber

general trend is captured well by FDNS. This indicates that the heat flux predictions from the code are qualitatively correct.

3.3.2 P&W Predictions

As a final benchmark of the FDNS code, the analysis for the 40K Nozzle (with film cooling) was performed, using the constant wall temperature of 1060R. This value was suggested as reasonable by P&W, and was the value used in their computations prepared for and distributed at the CFD consortium meeting in January, 1992. The original data supplied by P&W are shown in the Appendix.

Figure 3.6 shows a comparison of wall heat fluxes for the constant wall temperature case, with $T_w = 1060$R. The arrows at the base of the graph show the secondary and primary injection points. Note that FDNS predictions are slightly higher than those by P&W, but the trend is strongly reproduced.

3.4 Summary

3.4.1 Wall Jet

Parametric evaluation of the effect of inlet conditions of the wall jet of Holden [4] case 45 on the wall heat transfer yielded the following findings:

1. FDNS wall heat flux predictions are sensitive to velocity and temperature inlet profiles.
2. Use of constant over turbulent profiles yield acceptable, but not necessarily better, wall heat flux results.
3. Laminar inlet profiles produce unreasonable results for the wall heat flux downstream of the wall jet.

3.4.2 Combustor

Computation of the expansion of hot gases though a combustor in the configuration of the P&W 40K combustor yielded the following findings:

1. Higher values of turbulence kinetic energy at the inlet of the chamber, k_{inlet}, resulted in wall heat fluxes which more closely match those from hot firings [5].
2. All k_{inlet} values used resulted in overprediction of heat fluxes.

3.4.3 Subscale Nozzle - P&W Predictions

Computations for film cooling in the subscale nozzle for conditions similar to those used in computations performed by P&W resulted in the following findings:

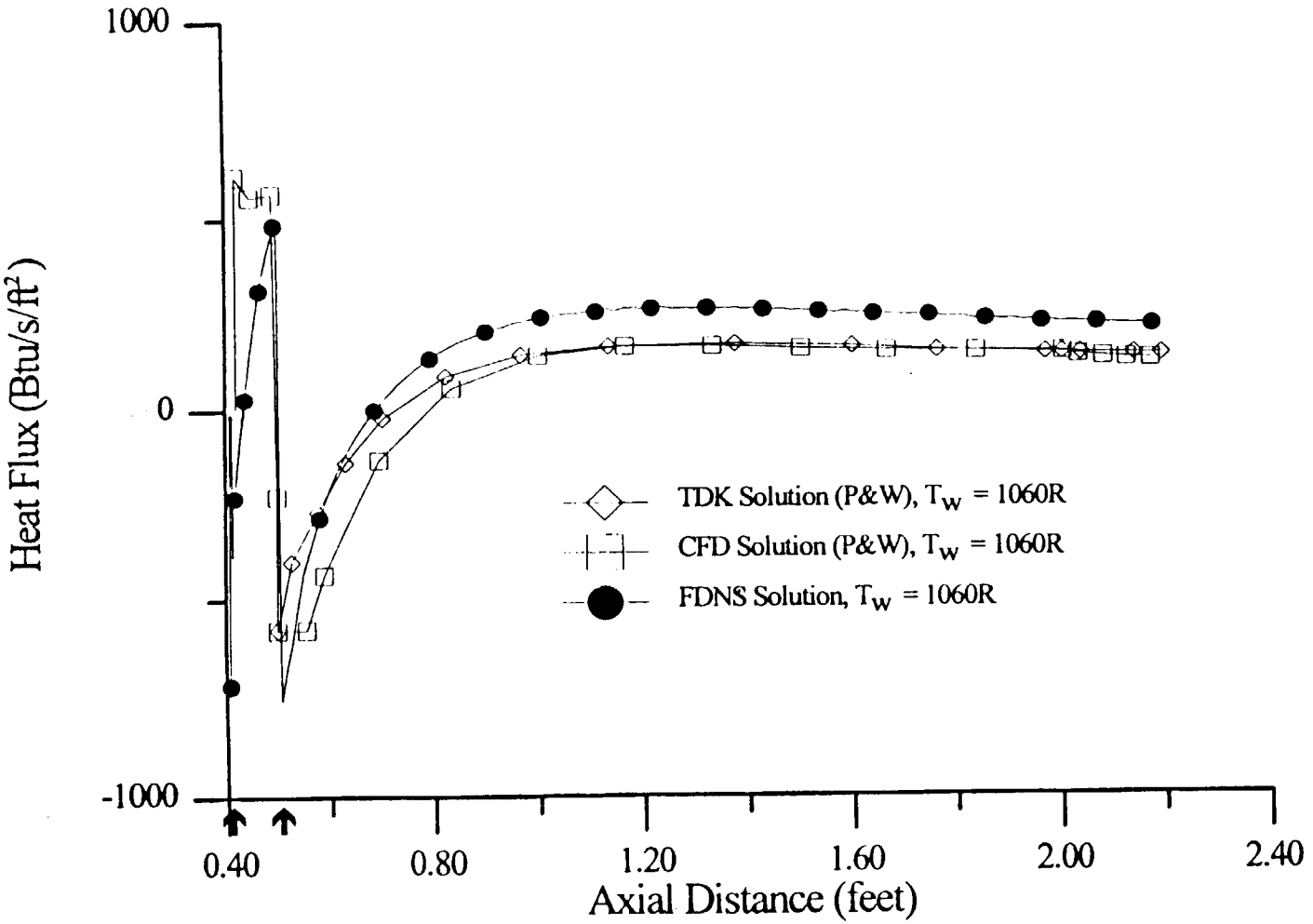

Figure 3.6: Comparison of FDNS Wall Fluxes with P&W Predictions for 40K Nozzle with constant Wall Temperature

1. FDNS closely reproduces computations by other methods.

2. FDNS overpredicts wall heat fluxes.

Chapter 4

The Conjugate Problem

4.1 Background

As alluded to previously, the FDNS program computes (via wall functions) heat fluxes corresponding to given wall temperatures. In order to have any type of predictive capability a means for determining the correct wall temperatures must be available.

The wall temperatures and corresponding heat fluxes are obviously not independent, but depend on the interaction at the wall surface between the hot gases flowing inside and whatever cooling mechanism is supplied on the back side of the wall. The task of simultaneously determining these two interface conditions, wall temperature and heat flux, based on complete specification of thermal boundary conditions on both sides of the wall, is known as a conjugate heat transfer problem.

(In the conceived Gas Generator Engine nozzle, the backside cooling will be supplied by partially combusted fuel flowing through channels parallel to the hot gas flow. In the 40K test article, the cooling will be supplied by water flowing through a calorimeter jacket. The 39 water cooling channels are cut perpendicular to the hot gas flow, so that the cooling water will flow circumferentially around the nozzle. Although this is drastically different from the flight article, this concept was chosen to allow for qualitative comparison of nozzle wall heat fluxes in the presence and absence of injected film coolant. *It should be emphasized that the wall temperatures, and resulting heat fluxes, are strongly dependent on the backside cooling mechanism.*)

In order to achieve a prediction for the wall temperatures, so that the heat fluxes could be obtained from FDNS, the conjugate heat transfer problem was solved iteratively by decoupling and matching conditions at the wall interface. This was accomplished by treating the wall heat flux as being fully one-dimensional at each location of the coolant channels, and applying simple heat exchanger theory to each coolant channel.

4.2 Theory

Figure 4.1 shows a single circumferential cooling channel above and below is the "heat exchanger model" of one such channel. At each axial location x, the heat flux was

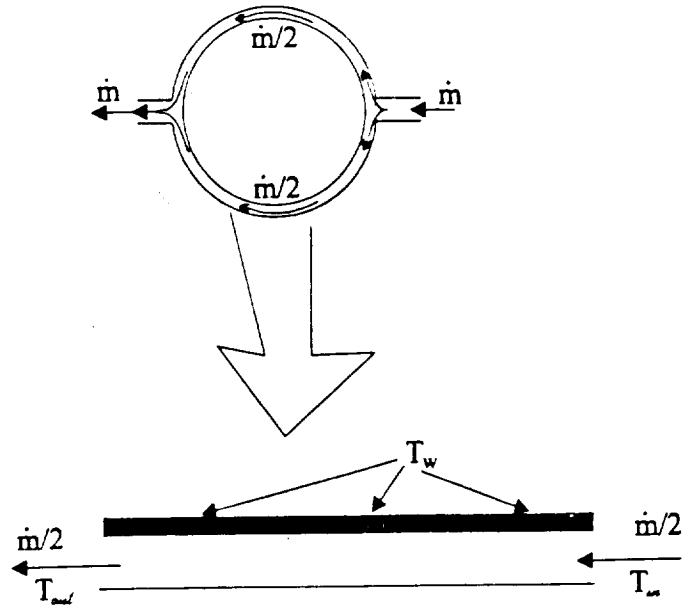

Figure 4.1: Treatment of Circumferential Cooling Channels

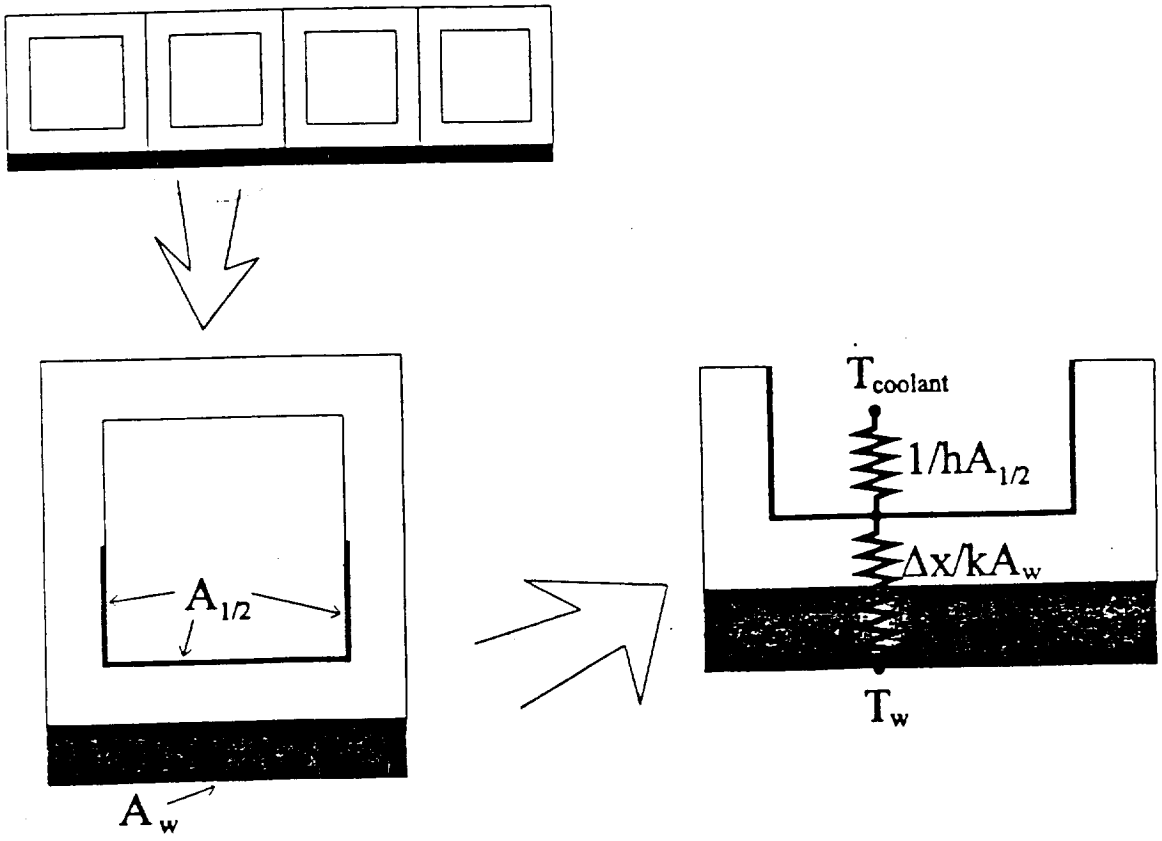

Figure 4.2: Overall Heat Transfer Coefficient for a Cooling Channel

assumed to be given by the heat exchanger relation

$$q'' = q/A = U\Delta T_{LM} \tag{4.1}$$

where U is the overall heat transfer coefficient, described by

$$UA = \frac{1}{\Sigma R_{th}} = \left[\frac{1}{h_w A_{1/2}} + \frac{\Delta x}{k A_w}\right]^{-1}. \tag{4.2}$$

In this relation, h_w is the usual heat transfer coefficient for water flowing in the channels, and $A_{1/2}$ is the surface area of one-half of the channel; Figure 4.2 shows the resistance concept for computation of the overall heat transfer coefficient U, along with some of the pertinent nomenclature. The area $A_{1/2}$ is consistent with the assumption that all the heat flow absorbed from one side of the channel. The required heat transfer coefficient can be computed if the water flow rate and average water temperature are known for each channel. The heat transfer coefficients were obtained from the Dittus-Boelter equation:

$$\mathrm{Nu} = 0.023\mathrm{Re}^{0.8}\mathrm{Pr}^{0.4}. \tag{4.3}$$

Here, both Nu and Re are based on the hydraulic diameter of the rectangular water flow passage. The second term in Equation 4.2 is the conduction term, and depends on the wall thickness Δx and the thermal conductivity k of the Inconel 625 nozzle liner material. A_w in this equation is the circumferential area of the landing below each cooling channel.

The water flow rates which were needed to compute the heat transfer coefficients were taken from drawings supplied by Pratt. These flow rates, and there axial locations, are shown in Table 4.1 below. There are two sets of water flow rates: the high one is for use during hot firings with no film coolant injection; the lower flow rates will be used when film cooling is used. Note that for each channel, the flow is divided at the inlet of the calorimeter jacket, and is reunited at the exit manifold (see Figure 4.1). This means that, for computing the heat transfer coefficients for each channel, only one-half the flow listed should be considered.

The term ΔT_{LM} in Equation 4.1 contains the wall surface temperature and this equation is what facilitates the uncoupling and iterative solution of the conjugate heat transfer problem. ΔT_{LM} is defined for a heat exchanger as the temperature difference at one end of the exchanger less the difference at the other end of the exchanger, divided by the natural logarithm of the ratio of the same two temperature differences. For the calorimeter jacket, each channel is modeled as a "heat exchanger", and the wall temperature at each x location is *assumed* to be constant around the perimeter of the nozzle. The lower portion of Figure 4.1 has the nomenclature. The temperature T_w must be determined for the given heat flux. For a constant wall temperature T_w, the log mean temperature difference ΔT_{LM} is given by

$$\Delta T_{LM} = \frac{(T_{out} - T_{in})}{\ln\left[(T_{out} - T_w)/(T_{in} - T_w)\right]}. \tag{4.4}$$

Channel Number	Axial Location inches	Low Flow lb/s	High Flow lb/s
1	7.057	0.255	1.000
2	7.557	0.255	1.060
3	8.057	0.255	1.095
4	8.557	0.255	1.100
5	9.057	0.270	1.100
6	9.557	0.280	1.083
7	10.057	0.300	1.055
8	10.557	0.325	1.020
9	11.057	0.360	0.980
10	11.557	0.400	0.940
11	12.057	0.400	0.870
12	12.557	0.400	0.820
13	13.057	0.400	0.780
14	13.557	0.400	0.735
15	14.057	0.400	0.695
16	14.557	0.400	0.660
17	15.057	0.400	0.620
18	15.557	0.400	0.600
19	16.057	0.400	0.565
20	16.557	0.400	0.540
21	17.057	0.400	0.520
22	17.557	0.400	0.500
23	18.057	0.400	0.480
24	18.557	0.400	0.460
25	19.057	0.400	0.447
26	19.557	0.390	0.432
27	20.057	0.380	0.420
28	20.557	0.370	0.405
29	21.057	0.360	0.392
30	21.557	0.355	0.381
31	22.057	0.340	0.378
32	22.557	0.340	0.362
33	23.057	0.330	0.355
34	23.557	0.320	0.345
35	24.057	0.315	0.338
36	24.557	0.310	0.330
37	25.057	0.300	0.320
38	25.557	0.295	0.315
39	26.057	0.290	0.305

Table 4.1: Water Flow Rates

The final relation needed to complete the decoupling is the temperature rise of the cooling water. This is the same as the equation which would be used to process the data from the calorimeter; that is

$$q = q''A = \dot{m}c_p(T_{out} - T_{in}) \tag{4.5}$$

4.3 Procedure

The procedure for the iterative solution of the conjugate heat transfer problem can now be outlined:

1. For the current distribution of wall surface temperatures, use the FDNS code to solve for the hot gas flow through the nozzle. An output of this solution is the wall heat flux corresponding to the given wall temperatures.

2. Based on the heat fluxes from step 1, use Equation 4.5 to compute the temperature rise of the water for each coolant channel.

3. Based on the water flow rate and temperature rise, determine h_w via Equation 4.3.

4. Compute the overall heat transfer coefficient UA (Equation 4.2).

5. Compute the wall temperature T_w using the current heat flux by combining Equations 4.1 and 4.4.

6. When the wall temperatures are sufficiently close to those used in step 1, STOP. Otherwise, return to step 1 and repeat using the newly computed wall temperatures.

Chapter 5

Task 3: Computed Results

As mentioned earlier, the results of the chamber analysis were used to establish the inlet condition to the calorimeter jacket. However, the results from the analysis of the chamber as used for test 027 could not be used directly, owing to modifications which are to be made to the chamber to accommodate the 40K nozzle. Specifically, before the nozzle will be mounted to the chamber, 1.500" will be cut from the head end of the combustor, and the tail end will be trimmed so that the overall length is 21.90". A new grid was generated corresponding to these modifications, and another analysis performed. All other conditions were held fixed: O/F=6.0, P_c = 1775 lb/in^2, $k_{inlet} = 0.1U^2$, and the same wall temperature distribution was impressed on the chamber wall as that reported by Dexter [5]. The results from this analysis were used as entry conditions to the 40K nozzle.

Lack of specific information about the cooling of the subscale nozzle outside of the range of the 39 coolant channels led to the adoption of *ad hoc* assumptions to facilitate the decoupling approach to the conjugate problem described earlier. Specifically, the entry to the nozzle is at axial location x = 4.90", and the first coolant channel is located at x = 7.057". For the no film cooling case, there will be no active cooling in this intermediate region; only radiative cooling to the atmosphere surrounding the test stand. For the film cooling case, there will be some back-side cooling provided by the coolant flowing though the nozzle manifold assembly. However, both of these scenarios present physics which cannot be easily incorporated into the framework of the decoupling approach to the conjugate problem outlined previously. As a patch to the solution methodology, the following simplifying assumption was made: the wall temperature varies smoothly and quadratically from a fixed temperature at x = 4.90" to the level of temperature at the first coolant channel at x = 7.057". This assumption allowed solutions to be obtained based on the previously outlined methodology.

5.1 No Film Cooling Case

The decoupling procedure described previously for solution of the conjugate problem converged quickly (in about four iterations). In this case, it was assumed that the wall temperature at the end of the chamber/beginning of the nozzle corresponded to the

same temperature as that measured by Dexter [5]. A quadratic interpolation scheme was used to fill in the missing temperature values up to the first cooling channel. The temperature was matched at the first cooling channel with an arbitrarily assumed zero slope.

The results of the iterations are seen in Figures 5.1 and 5.2. There are some non-physical oscillation in the heat flux in Figure 5.1 which are caused by too coarse mesh spacing upstream of the expansion at the (inactive) primary injection. From Figure 5.2, it can be seen that the maximum wall temperature is about 2200R, with an average wall temperature of about 1750R. This corresponds to a maximum heat flux (in the coolant channel section) of 750 Btu/ft^2/s (see Figure 5.1) , with an average wall heat flux in the coolant channel section of about 650 Btu/ft^2/s.

5.2 Film Cooled Case

The film cooled case used hydrogen gas supplied at ambient temperature (assumed 530R) at a pressure of 285 psi. Assuming isentropic expansion of the gas from the reservoir to the M=1.42 primary exit results in a static temperature of 376R, a static pressure of 86.2 psi, and a velocity of 5145 ft/s at the injector exit. For the exit area of the injectors, this corresponds to a mass flow rate of 0.02 lb/s for each injector, or a total flow rate of 2.68 lb/s for the 135 injectors.

Secondary coolant is supplied upstream of the supersonic film injectors to protect these nozzles from the hot gas flow. For an isentropic expansion to M=1, the temperature of the injected secondary coolant was 442R, and its velocity was 3905 ft/s. This corresponds to a mass flow rate of 0.50 lb/s for the secondary. The total flow rate simulated was 2.68 (primary) + 0.50 (secondary) = 3.18 lb/s.

A different set of *ad hoc* assumptions were used to substitute for inadequate knowledge of the backside cooling associated with the film delivery system. It was assumed that the temperature of the wall at the point of the secondary injection (the beginning of the nozzle section) was the temperature of the injected gas, about 520R. It was also assumed that the temperature of the wall at the point of the primary injection was the temperature of the cooling gas at this location, about 372R. Between these two stations, a "pseudo-adiabatic" condition was imposed through the iterative solution by forcing the wall temperature to equal the neighboring gas temperature. Between the primary injection and the first coolant channel, a quadratic variation of temperature was again used. Two different assumptions about the slope of the $T(x)$ function were tried: zero slope and constant slope based on the calorimeter jacket section.

The decoupling procedure for the film cooling case was non-convergent in this case. This is due to the inability of the simplistic quadratic interpolation procedure to substitute for the incomplete description of the physics. Figure 5.3 shows the last three iterations for the film cooled wall. The dashed lines are the temperatures and the solid lines are the heat transfer rates. The non-convergence is evident. *Note, however, that all the solutions give similar results in the water calorimeter channel section* where complete information on the backside cooling was available. It was

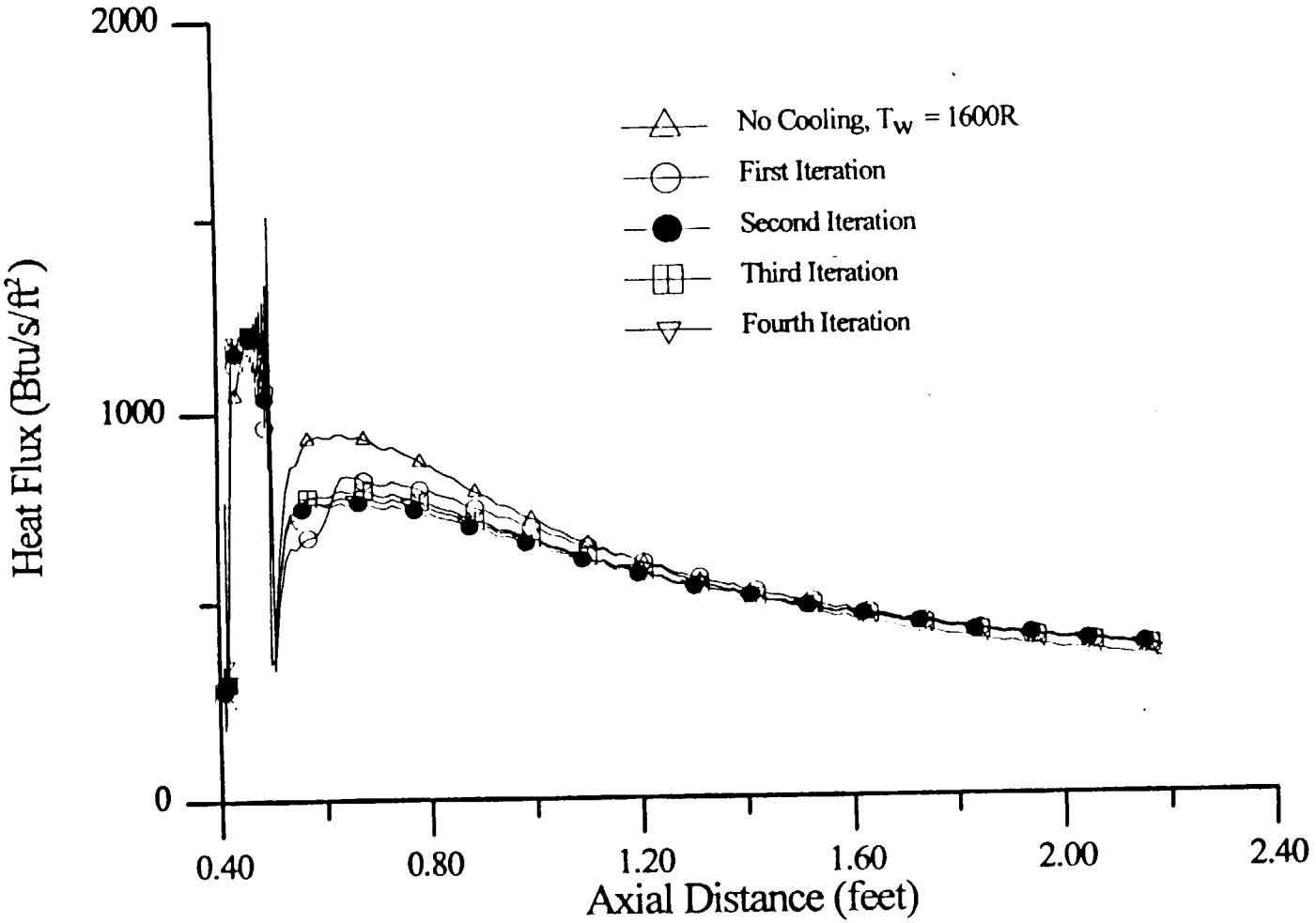

Figure 5.1: Iteration History (Fluxes) for Uncooled Nozzle

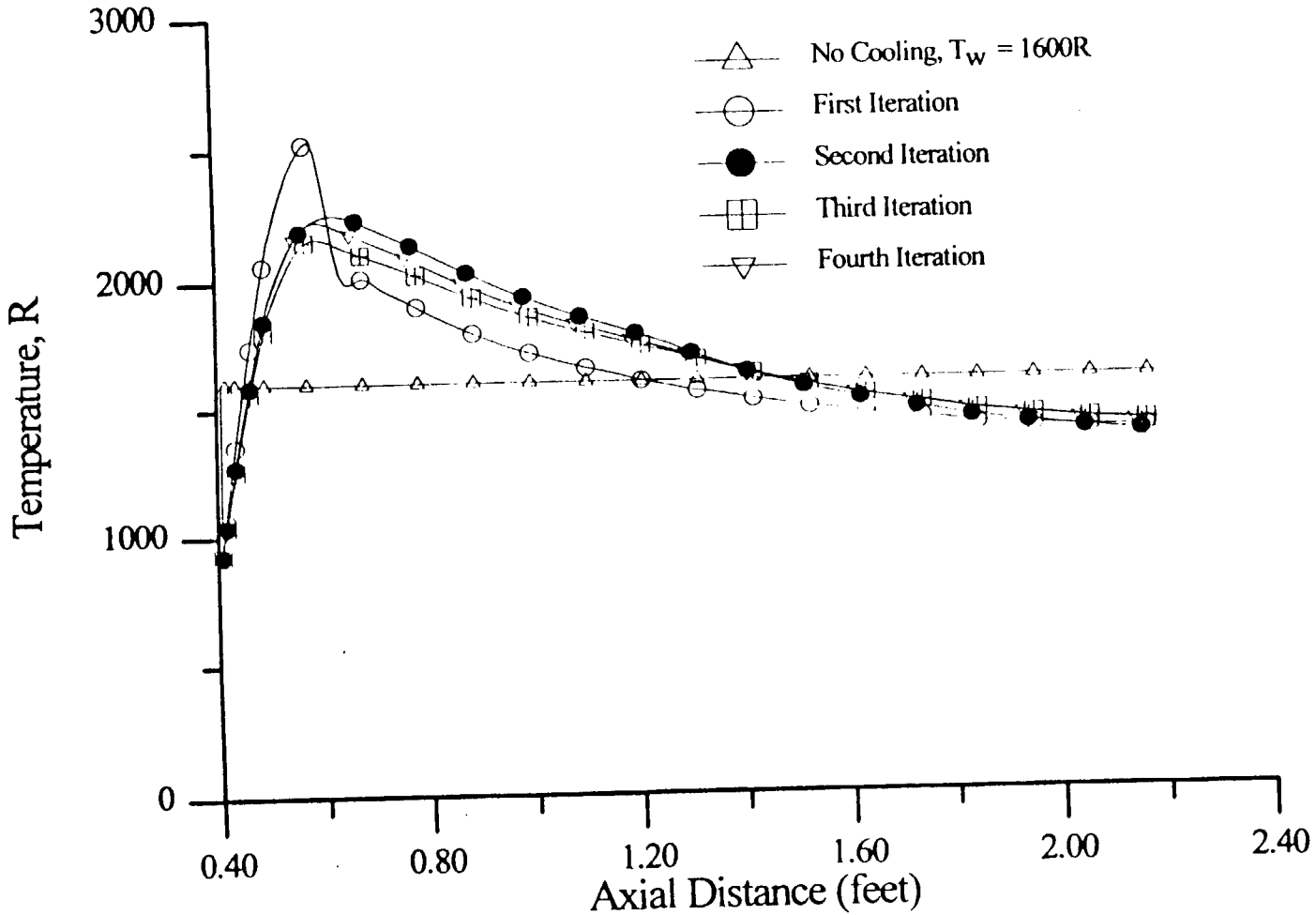

Figure 5.2: Iteration History (Temperatures) for Uncooled Nozzle

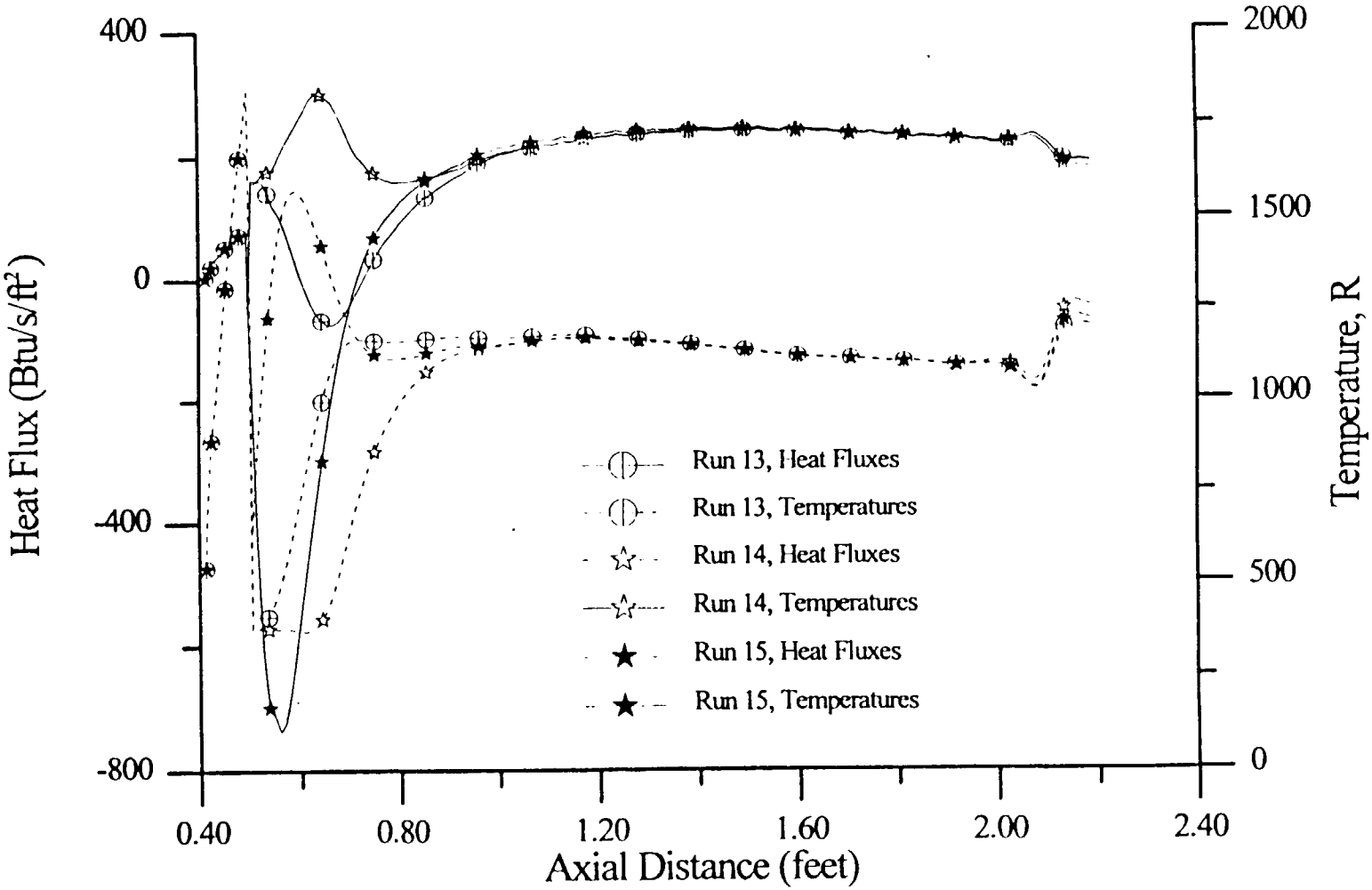

Figure 5.3: Last Three Iterations for Cooled Nozzle

apparent from the iterative process that a fixed number of candidate solutions had been exposed, as a repetitive cycle of solutions began to occur. Most of these could be dismissed on grounds of non-physical behavior. The solution from iteration 13 was deemed most plausible and will be considered correct for purposes of comparing with the uncooled wall case. For this case (iteration 13), the maximum wall temperature (in the coolant channel region) was about 1100R. The average temperature in this section was about 1050R. The wall heat fluxes varied from a slightly negative value (corresponding to wall cooling) to a maximum and nearly constant value of about 200 $Btu/ft^2/s$.

Note that although the predicted heat fluxes are felt to be too high, the converged value of wall temperature in the calorimeter section of 1050R is strikingly close to the value suggested by P&W (see Appendix). This would tend to suggest that the simple decoupling scheme, in conjunction with the FDNS heat flux predictions, yields accurate values of wall temperature, in spite of high heat flux predictions.

5.3 Comparison of Results

Figure 5.4 shows the results from the converged no cooling case with the selected film cooling case. The dramatic difference in these results shows the advantage which can be expected by using film cooling.

Figure 5.5 shows the color contours of temperature of the hot gas flow when no film cooling is used. Figure 5.6 presents the temperature contours for the case where film cooling is used. Note that for the uncooled case, the temperature contours are nearly one-dimensional in the axial direction. The addition of film cooling creates an annular cooled buffer at the wall, as desired, but the one-dimensional axial core is retained.

Figure 5.7 shows the computed hydrogen concentration contours, and Figure 5.8 provides a detail of the injector region. It is clear that the injected hydrogen penetrates to about 1/3 of the nozzle radius with a concentration of 0.40 or greater. Note that the core flow, which is not affected by the film coolant, has a hydrogen concentration of about 0.25.

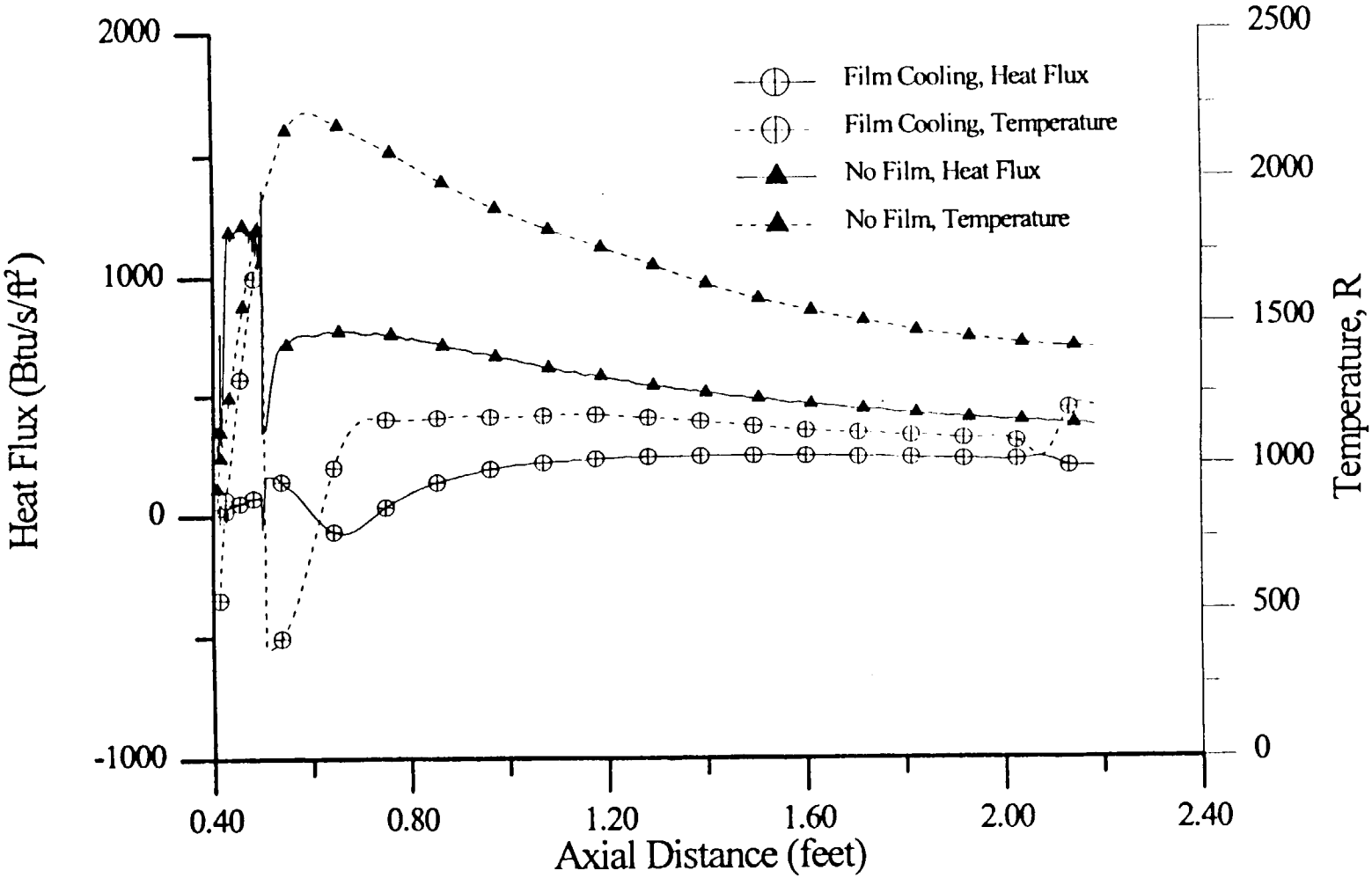

Figure 5.4: Comparison of Cooled and Uncooled Nozzle Conditions

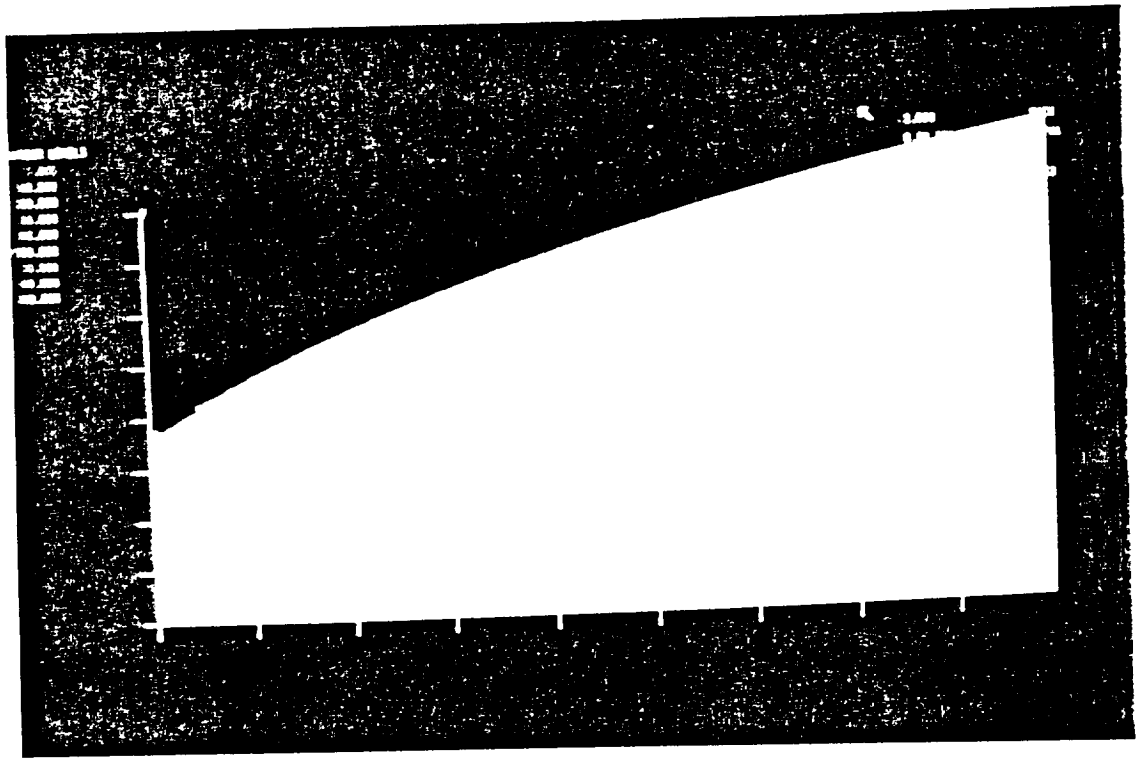

Figure 5.5: Temperature Contours for No Film Cooling

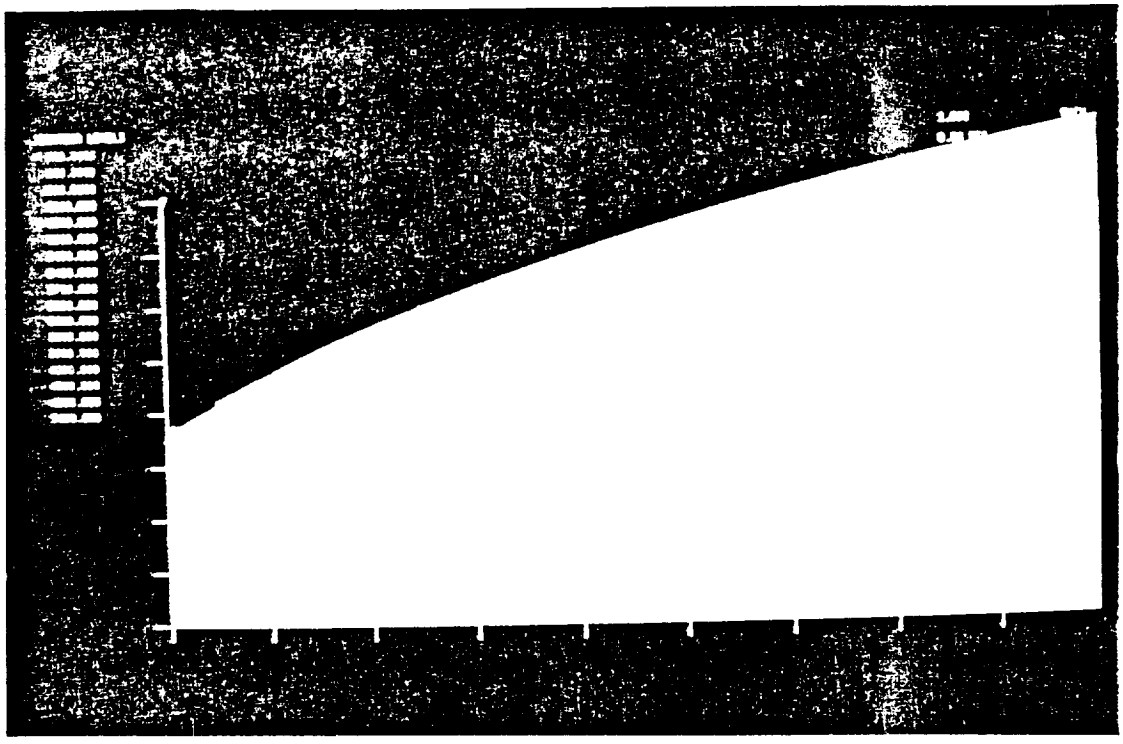

Figure 5.6: Temperature Contours with Film Cooling

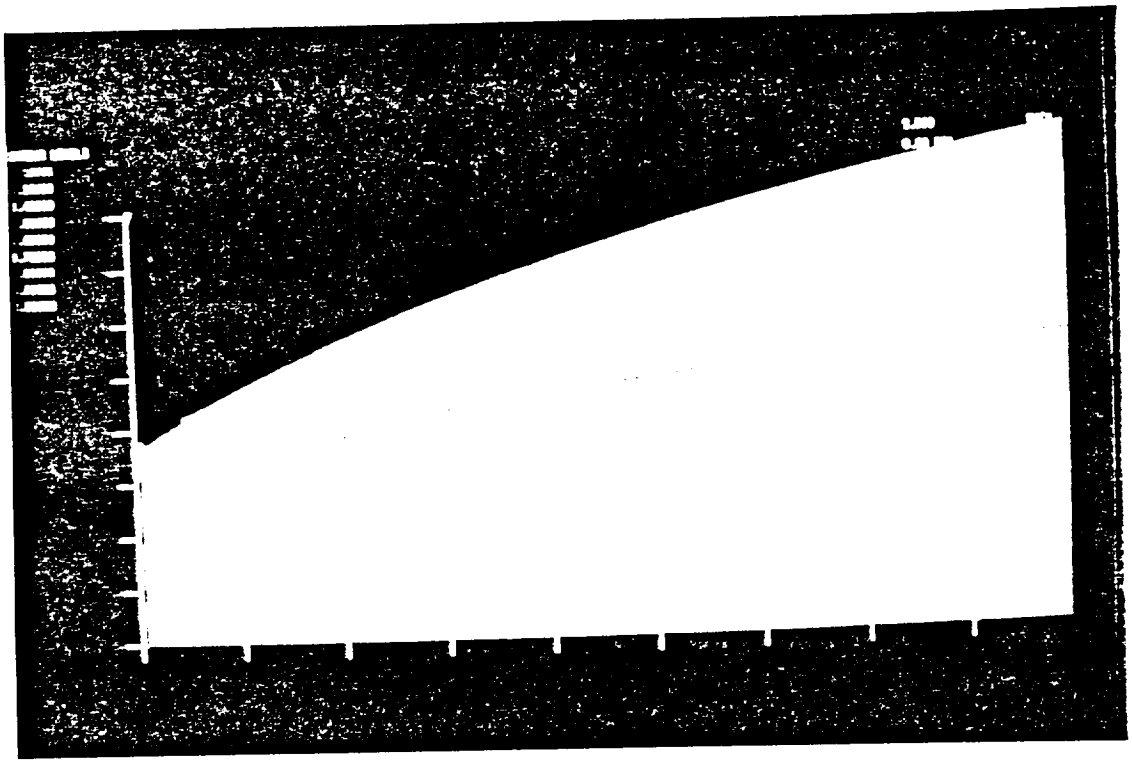

Figure 5.7: Hydrogen Contours for Film Cooling

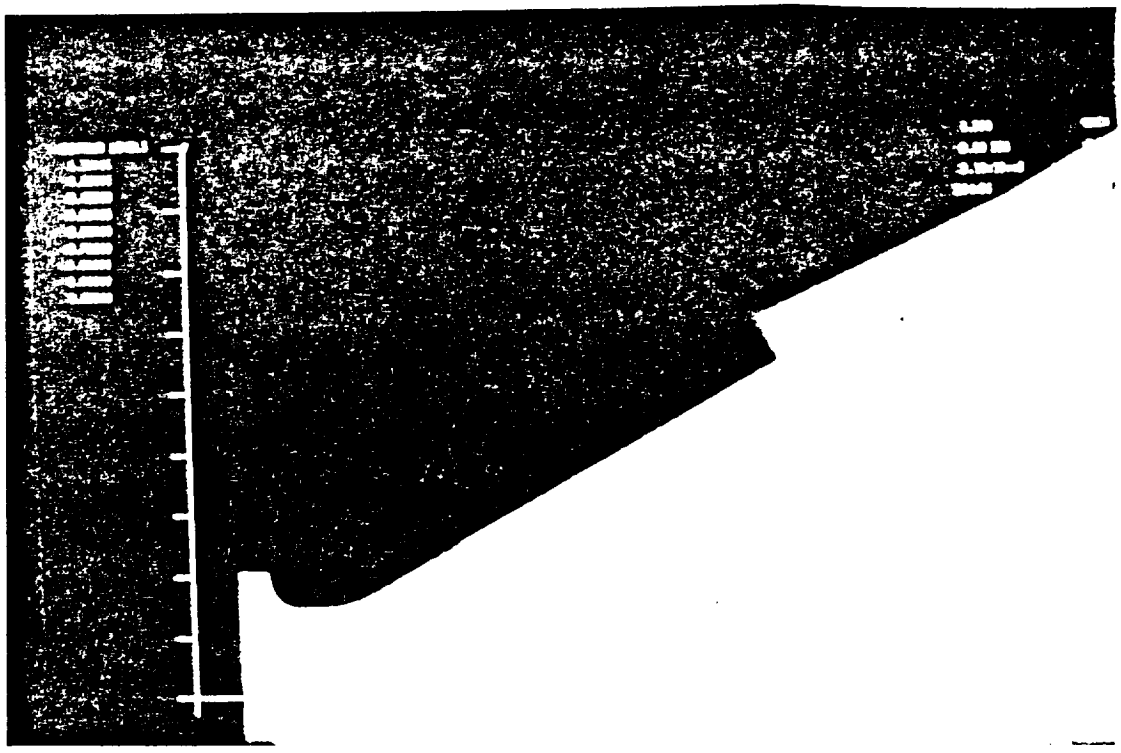

Figure 5.8: Hydrogen Contours for Film Cooling: Injection Detail

Chapter 6

Summary

1. The Reynolds Analogy-based wall function gives reasonable, but not accurate, estimates of the wall heat flux downstream of a wall jet.

2. The predictions obtained depend on the velocity and temperature profiles of the flow at the injection. However, uniform profiles give as good agreement as any other assumption (turbulent, or laminar). Of course, actual inlet profiles will produce more accurate results.

3. The inlet velocity profile affects wall heat flux much more than the temperature profile does.

4. The FDNS program tends to overpredict heat fluxes, but gives excellent qualitative agreement with experimental data and good agreement with other computational predictions.

5. For the no film cooled case, the predicted maximum temperature in the calorimeter jacket section is 2200R, and the average temperature is about 1750R.

6. For the no film cooled case, the predicted maximum heat flux in the calorimeter jacket section is 750 $Btu/ft^2/s$, with an average wall heat flux of about 650 $Btu/ft^2/s$.

7. For the film cooled case, the predicted maximum temperature in the calorimeter jacket section is 1100R, and the average temperature is about 1050R.

8. For the film cooled case, the predicted heat flux in the calorimeter jacket section varied from a slightly negative value to a maximum and nearly constant value of about 200 $Btu/ft^2/s$.

9. The simple decoupling procedure applied to handle the conjugate heat transfer problem yields results for the cooled nozzle liner temperature in agreement with values suggested by P&W. With more accurate information about the backside cooling, this procedure could be used to predict wall temperatures in other film cooling applications.

Bibliography

[1] B. E. Launder and D. B. Spalding, "Numerical computation of turbulent flows," *Computer Methods in Applied Mechanics and Engineering*, vol. 3, pp. 269–289, 1974.

[2] K. A. Woodbury, "Assessment of nasa code FDNS2D for computation of film cooling effectiveness," Tech. Rep. ZZ, NASA/ASEE SFFP, August 1991. prepared for NASA/MSFC, Contract NGT-01-008-021.

[3] C. P. Chen, "Benchmark problem: Status report." Presented at CFD Consortium Meeting, NASA/MSFC, August 1 1991.

[4] M. S. Holden, "A data base of experimental studies of shock wave/wall jet interaction in hypersonic flow," tech. rep., Calspan-UB Research Center, Buffalo, NY, April 1990.

[5] C. Dexter, "Private communication." MSFC, Huntsville, AL, August 1992.

[6] A. H. Shapiro, *The Dynamics and Thermodynamics of Compressible Flow.* Brown, 1954.

[7] M. S. Holden, "Shock wave-turbulent boundary layer interaction in hypersonic flow," Tech. Rep. 77-45, AIAA, January 24-26 1977. presented at AIAA 15th Aerospace Sciences Meeting.

[8] Y. S. Chen, "FDNS user's short course." held at ESI, Huntsville, AL, July 1992.

Appendix A: Dexter Data

P242-027 t= 15.035

P1088 - 1741
TCA Pc P1089 - 1746 ave. = 1760 + 15 = 1775
P1090 - 1766
Wall Static Pc P1093 - 1770
P1094 - 1775

LOX SYSTEM

TANK P0001 - 3116
VENT P1004 - 3073
P1005 - 3069 Ave. = 3071 + 15 = 3086
VALVE P1062 - 1933
LOX DOME P1060 - 1903
P1061 - 1853 > 1878 + 15 = 1893

T0077 - -266
T1001 - -263
T1006 - -261
T1076 - -310 (BAD)

VENTURI DIA. = .4872 A = .1864 Cd = .96

w/CdA = 298.0 @ P = 3086, T = -262

wLox = 298.0(.1864)(.96) = 53.33

H2 SYSTEM

TANK P0002 - 3330
GH2 MIXER INLET P1001 - 3330
MIXER INLET P1011 - 3269
MIXER OUTLET P1037 - 3320

T1004 - -264
T1014 - -272
T1012 - -267

VENT IN P1006 - 3236
P1007 - 3267 Ave. = 3252 + 15 = 3267
VENT OUT P1035 - 2009
FUEL MANIFOLD P1073 - 1978
FUEL CAVITY P1091 - 1939
P1092 - 1942 > 1941 + 15 = 1956

T1075 - BAD (-262)

VENTURI DIA. = .583 A = .2669 Cd = .968

w/CdA = 34.4 @ P = 3267, T = -267

wH2 = 34.4(.2669)(.968) = 8.89

O/F = 53.33/8.89 = 6.00

C* = 1775(32.2)(8.3725)/53.33 + 8.89 = 7690.9

nC = 7690.9

PRATT WHITN .0K P242-027

P1051 = 4402 Plog = 4399 P242-027 T1010- 72.90
P1054 = 4396 t = 15.035 T1011- 73.20

CH NO.	Aflow in2	As in2	Orif No.	F/M NO.	w F/M	PRESS NO.	P Orif	TEMP NO.	K	w * base	Vc	T at t=0	TOUT	Delta T	w scaled	Q/A	
1	0.0191	6.389	86					T1105	0.049	3.25	196	76.3	79.3	3	3.25	1.53	
2	0.0192	6.41	87					T1085	0.047	3.12	187	74.5	90.4	15.9	3.12	7.73	Type J
3	0.0189	6.396	88					T1051	0.047	3.12	190			####	3.12	####	Type J
4	0.0188	6.399	103					T1097	0.05	3.32	204	75.5	114.2	38.7	3.32	20.06	Type J
5	0.0188	6.395	124	F1007	2.62	P1014	4345	T1053	0.04	2.65	163	75.7	119.5	43.8	2.65	18.17	
6	0.0188	6.402	115					T1115	0.047	3.12	191	76.9	123.2	46.3	3.12	22.54	
7	0.0188	6.402	116					T1052	0.05	3.32	204	75.5	132.8	57.3	3.32	29.68	Type J
8	0.0189	6.409	121					T1102	0.042	2.79	170	75.7	134	58.3	2.79	25.34	
9	0.0189	6.398	128	F1025	3.04	P1012	3245	T1106	0.046	3.05	186	76.5	133.3	56.8	3.05	27.09	
10	0.019	6.398	129					T1091	0.05	3.32	201	75.7	130.9	55.2	3.32	28.61	
11	0.019	6.398	130					T1098	0.048	3.18	193	76.4	131.1	54.7	3.18	27.22	Type J
12	0.0095	3.192	123					T1049	0.024	1.59	193	75.7	139.1	63.4	1.59	31.62	Type J
13	0.0268	7.372	125	F1019	3.05	P1042	3908	T1042	0.046	3.05	131	74.2	156.8	82.6	3.05	34.18	Type J
14	0.0266	7.095	132					T1120	0.053	3.52	152			####	3.52	####	
15	0.0264	7.113	133					T1059	0.053	3.52	154	74.9	130.7	55.8	3.52	27.58	
16	0.0265	7.11	134	F1026	3.43	P1020	3714	T1045	0.052	3.45	150	75.6	134.4	58.8	3.45	28.52	
17	0.0265	7.116	135					T1107	0.049	3.25	142	75.4	134.2	58.8	3.25	26.85	
18	0.0265	7.11	136					T1092	0.049	3.25	142	75.4	135	59.6	3.25	27.24	
19	0.0265	7.106	137	F1010	3.43	P1023	3820	T1047	0.051	3.38	147	74.8	132.3	57.5	3.38	27.37	
20	0.0264	7.113	138					T1100	0.052	3.45	151	75	129.7	54.7	3.45	26.52	

CH NO.	Aflow in2	As in2	Orif No.	F/M NO.	w F/M	PRESS NO.	P Orif	TEMP NO.	K	w * base	Vc	T at t=0	TOUT	Delta T	w scaled	Q/A	
21	0.0264	7.113	161					T1043	0.049	3.25	142	71.8	139.2	67.4	3.25	30.79	Type J
22	0.0265	7.107	140	F1021	3.48	P1044	3714	T1086	0.052	3.45	150	75.1	129.6	54.5	3.45	26.45	Type J
23	0.0265	7.111	149					T1110	0.051	3.38	147	73.4	137	63.6	3.38	30.25	
24	0.0265	7.114	150					T1048	0.05	3.32	144	75.6	128.3	52.7	3.32	24.57	
25	0.0265	7.11	151					T1108	0.05	3.32	144	75	129.6	54.6	3.32	25.47	
26	0.0265	6.672	152	F1002	3.40	P1021	3723	T1093	0.05	3.32	144	75.4	125.9	50.5	3.32	25.10	
27	0.0156	3.903	111					T1050	0.041	2.72	201	74.6	117.9	43.3	2.72	30.17	Type J
28	0.0157	3.915	108					T1124	0.041	2.72	200	76.2	112.7	36.5	2.72	25.35	
29	0.0158	3.907	109	F1003	2.47	P1017	3187	T1044	0.039	2.59	189	76.5	113.3	36.8	2.59	24.36	
30	0.0158	3.898	104					T1056	0.044	2.92	213	77.1	109.4	32.3	2.92	24.18	
31	0.0161	3.876	127					T1111	0.043	2.85	204	76.7	111.5	34.8	2.85	25.61	
32	0.0161	3.869	171	F1006	2.79	P1015	3100	T1046	0.042	2.79	200	76.6	111.1	34.5	2.79	24.84	
33	0.0161	3.855	172					T1088	0.043	2.85	204	76.7	113.7	37	2.85	27.37	
34	0.0161	3.828	173					T1094	0.042	2.79	200	76.6	112.6	36	2.79	26.20	
35	0.0152	3.783	164	F1028	2.84	P1024	2984	T1099	0.042	2.79	211	77	112.4	35.4	2.79	26.07	
36	0.0152	3.781	165	F1027	2.92	P1027	2826	T1125	0.045	2.98	227	77.6	113.2	35.6	2.98	28.10	
37	0.0152	3.753	166					T1089	0.044	2.92	222	77.4	112.9	35.5	2.92	27.60	
38	0.0151	3.714	167	F1029	2.70	P1025	3090	T1114	0.041	2.72	208	76.7	116.8	40.1	2.72	29.36	
39	0.0152	3.683	174					T1112	0.043	2.85	217	75.8	115.9	40.1	2.85	31.05	
40	0.0152	3.643	175					T1090	0.042	2.79	211	77.1	115.7	38.6	2.79	29.52	

CH NO.	Aflow in2	As in2	Orif No.	F/M NO.	w F/M	PRESS NO.	P Orif	TEMP NO.	K	w * base	Vc	T at t=0	TOUT	Delta T	w scaled	Q/A	
41	0.0169	3.6	153	F1030	3.20	P1026	2845	T1109	0.047	3.12	213	77.4	114.1	36.7	3.12	31.78	
42	0.0168	3.556	163					T1095	0.048	3.18	219	77.2	115.3	38.1	3.18	34.11	
43	0.0167	3.503	39					T1087	0.051	3.38	234	77.7	113.4	35.7	3.38	34.47	
44	0.0166	3.446	30	F1001	3.53	P1019	2579	T1104	0.053	3.52	244	78	113.5	35.5	3.52	36.21	
45	0.0166	3.379	36					T1116	0.055	3.65	254	78.5	113.1	34.6	3.65	37.35	
46	0.017	3.328	91	F1016	3.70	P1031	2573	T1055	0.056	3.71	252	78.4	114.6	36.2	3.71	40.40	
47	0.0171	3.266	34	F1013	3.86	P1018	2330	T1122	0.058	3.85	260	78.7	113.4	34.7	3.85	40.87	
48	0.0168	3.194	17	F1017	3.51	P1038	2638	T1118	0.055	3.65	251	76.9	120.8	43.9	3.65	50.14	Type J
49	0.0173	3.118	29					T1057	0.06	3.98	265	78.5	122.7	44.2	3.98	56.41	Type J
50	0.017	3.04	72	F1018	3.90	P1041	2322	T1096	0.059	3.91	266	78.8	115.9	37.1	3.91	47.76	
51	0.0167	2.963	75					T1066	0.06	3.98	275	78.9	116.4	37.5	3.98	50.36	
52	0.0166	2.871	70	F1020	3.94	P1030	2296	T1062	0.06	3.98	277	79	117.5	38.5	3.98	53.36	
53	0.0168	2.797	77					T1103	0.057	3.78	260	78.4	119.5	41.1	3.78	55.55	
54	0.0165	2.69	80	F1031	4.09	P1016	2264	T1101	0.061	4.05	283	79	117.9	38.9	4.05	58.51	
55	0.0163	2.604	66	F1009	3.79	P1028	2452	T1060	0.058	3.85	272	78.7	119.6	40.9	3.85	60.42	
56	0.016	2.476	35	F1014	3.66	P1032	2655	T1121	0.055	3.65	263	77.9	116.4	38.5	3.65	56.72	
57	0.0157	2.356	62					T1083	0.059	3.91	288	79.1	112.1	33	3.91	54.81	
58	0.0153	2.275	69	F1023	3.95	P1033	2121	T1123	0.059	3.91	295	79.1	108.6	29.5	3.91	50.74	
59	0.0155	2.263	37	F1008	3.58	P1034	2540	T1054	0.053	3.52	262	78.4	110	31.6	3.52	49.09	
60	0.0152	2.404	43					T1126	0.064	4.25	322	80.2	104.9	24.7	4.24	43.61	Type J

CH NO.	Aflow In2	As In2	Orif No.	F/M NO.	w F/M	PRESS NO.	P Orif	TEMP NO.	K	w * base	Vc	T at t=0	TOUT	Delta T	w scaled	Q/A	
61	0.015	2.833	21	F1011	4.09	P1029	1584	T1063	0.06	3.98	306	80.4	100.4	20	3.98	28.09	Type J
62	0.0152	3.089	23					T1113	0.063	4.18	317			####	4.18	####	Type J
63	0.0226	5.378	45					T1058	0.078	5.17	264	80	101.4	21.4	5.17	20.59	
64	0.0223	6.285	58	F1012	4.41	P1039	2504	T1119	0.068	4.51	233	77.7	109.4	31.7	4.51	22.75	Type J
65	0.0227	7.096	15					T1064	0.069	4.58	233	79.5	111.7	32.2	4.58	20.77	Type J
66	0.0285	8.138	176	F1015	2.85	P1043	3891	T1065	0.042	2.79	113	74.8	115.9	41.1	2.79	14.07	
67	0.0282	8.838	117					T1041	0.038	2.52	103	74.7	119.1	44.4	2.52	12.66	
68	0.0283	9.525	119					T1061	0.044	2.92	119	74.7	113.5	38.8	2.92	11.89	
69	0.0281	10.227	107	F1004	2.88	P1022	3980	T1117	0.044	2.92	120	74.5	110.9	36.4	2.92	10.39	
70	0.0276	10.93	168					T1081	0.041	2.72	114	74.1	111.8	37.7	2.72	9.38	
71	0.0271	11.621	169					T1082	0.039	2.59	110	76.1	121.8	45.7	2.59	10.17	Type J
72	0.0271	12.318	170	F1022	2.67	P1045	3902	T1084	0.04	2.65	113	74.8	113.8	39	2.65	8.40	

P&W 40K Subscale Calorimeter Chamber and Heat Flux Data

Channel No.	Axial Location	Wall Radius	Land Width	No. of Passages	Passage Width	Surface Width (1)	Surface Area (2)	Test 027C Q/A	Test 027C Q	Test 027C Wall Temp (R)
1	-16.702	2.8291	0.1078	2	0.0719	0.3594	6.39	1.5	9.58	582
2	-16.342	2.8291	0.1082	2	0.0721	0.3606	6.41	7.7	49.36	757
3	-15.982	2.8291	0.1085	2	0.0714	0.3598	6.40	11.2	71.63	
4	-15.622	2.8291	0.1086	2	0.0714	0.36	6.40	14.7	94.07	
5	-15.262	2.8289	0.1089	2	0.071	0.3598	6.40	18.2	116.39	1048
6	-14.902	2.8287	0.1093	2	0.0708	0.3602	6.40	22.5	144.04	1138
7	-14.542	2.8286	0.109	2	0.0711	0.3602	6.40	23.9	153.00	
8	-14.182	2.8287	0.109	2	0.0713	0.3606	6.41	25.3	162.15	1230
9	-13.822	2.8284	0.1087	2	0.0713	0.36	6.40	27.1	173.38	1259
10	-13.462	2.8284	0.1081	2	0.0719	0.36	6.40	28.6	182.97	1282
11	-13.102	2.8286	0.1081	2	0.0719	0.36	6.40	27.2	174.03	1255
12	-12.832	2.8288	0.1075	1	0.0721	0.1796	3.19	27.4	87.47	
13	-12.532	2.8287	0.1053	2	0.1021	0.4148	7.37	27.4	202.00	
14	-12.127	2.8287	0.0983	2	0.1013	0.3992	7.10	27.4	194.41	
15	-11.727	2.8286	0.0994	2	0.1007	0.4002	7.11	27.6	196.31	1292
16	-11.327	2.8289	0.0989	2	0.1011	0.4	7.11	28.5	202.63	1320
17	-10.927	2.8287	0.0989	2	0.1013	0.4004	7.12	26.8	190.72	1289
18	-10.527	2.8291	0.0986	2	0.1014	0.4	7.11	27.2	193.40	1299
19	-10.127	2.8289	0.0987	2	0.1012	0.3998	7.11	27.4	194.71	1294
20	-9.727	2.8289	0.099	2	0.1011	0.4002	7.11	26.5	188.50	1269
21	-9.327	2.8287	0.0989	2	0.1012	0.4002	7.11	26.5	188.49	
22	-8.927	2.8293	0.0984	2	0.1015	0.3998	7.11	26.5	188.34	1265
23	-8.527	2.8293	0.0982	2	0.1018	0.4	7.11	25.55	181.68	
24	-8.127	2.8292	0.0983	2	0.1018	0.4002	7.11	24.6	175.01	1226
25	-7.727	2.8291	0.0982	2	0.1018	0.4	7.11	25.2	179.18	1205
26	-7.327	2.8288	0.0859	2	0.1018	0.3754	6.67	25.85	172.48	
27	-7.041	2.8289	0.05	2	0.0598	0.2196	3.90	26.5	103.44	1140
28	-6.821	2.8272	0.0498	2	0.0604	0.2204	3.92	25.8	101.01	1125
29	-6.601	2.823	0.0494	2	0.0607	0.2202	3.91	24.5	95.69	1100
30	-6.381	2.8162	0.0492	2	0.0609	0.2202	3.90	25.8	100.53	1116
31	-6.161	2.807	0.0478	2	0.062	0.2196	3.87	25.3	97.99	1110
32	-5.941	2.795	0.0478	2	0.0622	0.22	3.86	26.7	103.16	1145
33	-5.721	2.7803	0.0477	2	0.0624	0.2202	3.85	26.6	102.32	1139
34	-5.501	2.7632	0.0476	2	0.0623	0.2198	3.82	26	99.22	1131
35	-5.281	2.7434	0.0502	2	0.0591	0.2186	3.77	26.6	100.23	1141
36	-5.061	2.7208	0.0509	2	0.0591	0.22	3.76	27.9	104.93	1158
37	-4.841	2.6966	0.0509	2	0.0592	0.2202	3.73	30.6	114.17	1212
38	-4.621	2.6697	0.0507	2	0.0592	0.2198	3.69	28.7	105.82	1177
39	-4.401	2.6393	0.0505	2	0.0595	0.22	3.65	30.9	112.73	1214
40	-4.181	2.6062	0.0505	2	0.0595	0.22	3.60	29.5	106.28	1190
41	-3.961	2.5705	0.0505	2	0.0595	0.22	3.55	31.8	112.99	1117
42	-3.741	2.532	0.0507	2	0.0594	0.2202	3.50	34.1	119.46	1152
43	-3.521	2.4909	0.0508	2	0.0592	0.22	3.44	34.5	118.79	1148
44	-3.301	2.4468	0.0509	2	0.059	0.2198	3.38	36.2	122.32	1169
45	-3.081	2.4002	0.0505	2	0.0591	0.2192	3.31	37.3	123.30	1180

46	-2.861	2.3507	0.0493	2	0.0606	0.2198	3.25	40.4	131.16	1227
47	-2.641	2.2984	0.0489	2	0.0611	0.22	3.18	40.9	129.94	1229
48	-2.421	2.2342	0.0498	2	0.0601	0.2198	3.09	43.2	133.29	
49	-2.201	2.1853	0.0496	2	0.0602	0.2196	3.02	45.4	136.89	
50	-1.981	2.1249	0.0505	2	0.0593	0.2196	2.93	47.7	139.85	1277
51	-1.761	2.0616	0.0512	2	0.0587	0.2198	2.85	50.4	143.50	1309
52	-1.541	1.995	0.051	2	0.0586	0.2192	2.75	53.4	146.73	1350
53	-1.321	1.9254	0.0504	2	0.0598	0.2204	2.67	55.6	148.25	1394
54	-1.101	1.8531	0.0511	2	0.059	0.2202	2.56	58.3	149.47	1411
55	-0.881	1.7771	0.0515	2	0.0587	0.2204	2.46	60.4	148.64	1456
56	-0.661	1.7101	0.0515	2	0.0587	0.2204	2.37	56.7	134.28	1410
57	-0.441	1.6647	0.0514	2	0.0589	0.2206	2.31	54.8	126.45	1364
58	-0.221	1.6391	0.0514	2	0.0583	0.2194	2.26	51.95	117.38	
59	-0.001	1.6336	0.0516	2	0.0586	0.2204	2.26	49.1	111.08	1302
60	0.219	1.6897	0.051	2	0.0587	0.2194	2.33	43.6	101.56	1214
61	0.439	1.8069	0.0503	2	0.0598	0.2202	2.50	28.1	70.25	1006
62	0.659	1.9342	0.0504	2	0.0596	0.22	2.67	24.35	65.10	
63	0.939	2.0967	0.058	2	0.0597	0.2354	3.10	20.6	63.88	953
64	1.309	2.3112	0.0654	2	0.0594	0.2496	3.62	18.4	66.69	
65	1.684	2.5286	0.0686	2	0.0602	0.2576	4.09	16.3	66.71	
66	2.0865	2.7618	0.0896	2	0.1133	0.4058	7.04	14.1	99.29	1042
67	2.4925	2.9972	0.0907	2	0.1123	0.406	7.65	12.7	97.10	1002
68	2.8985	3.2324	0.091	2	0.1119	0.4058	8.24	11.9	98.08	973
69	3.3045	3.4679	0.0906	2	0.1124	0.406	8.85	10.4	92.00	940
70	3.7105	3.7036	0.091	2	0.1121	0.4062	9.45	9.4	88.85	929
71	4.1165	3.9394	0.091	2	0.112	0.406	10.05	8.9	89.44	
72	4.5225	4.1749	0.091	2	0.1121	0.4062	10.66	8.4	89.50	925
							Total Q (Btu/sec) =		9095.67	

Q (Btu/sec) to Throat = 8007.2

Note 1: Surface width = No. of passages (land width + passage width)
Note 2: Surface Area = 2 pi (surface width)(wall radius)

P242-027 HEAT FLUX

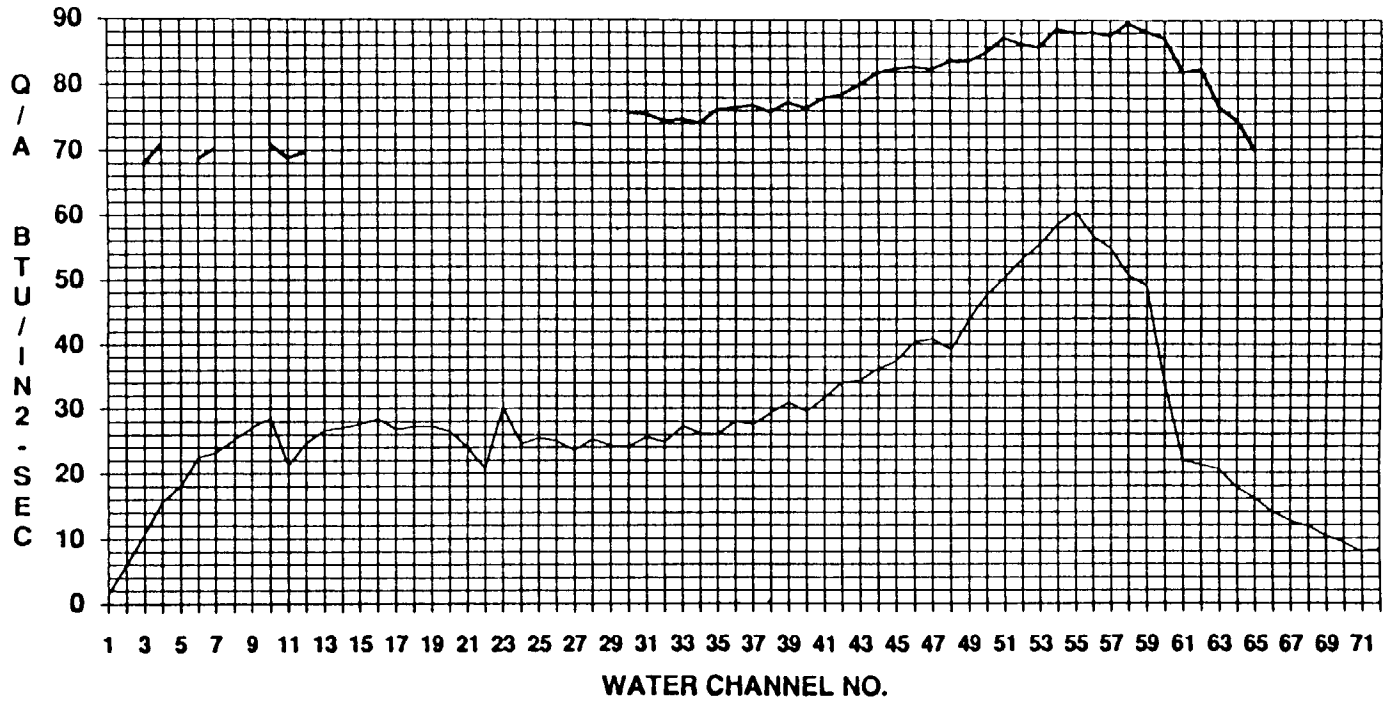

P242-027 HEAT FLUX

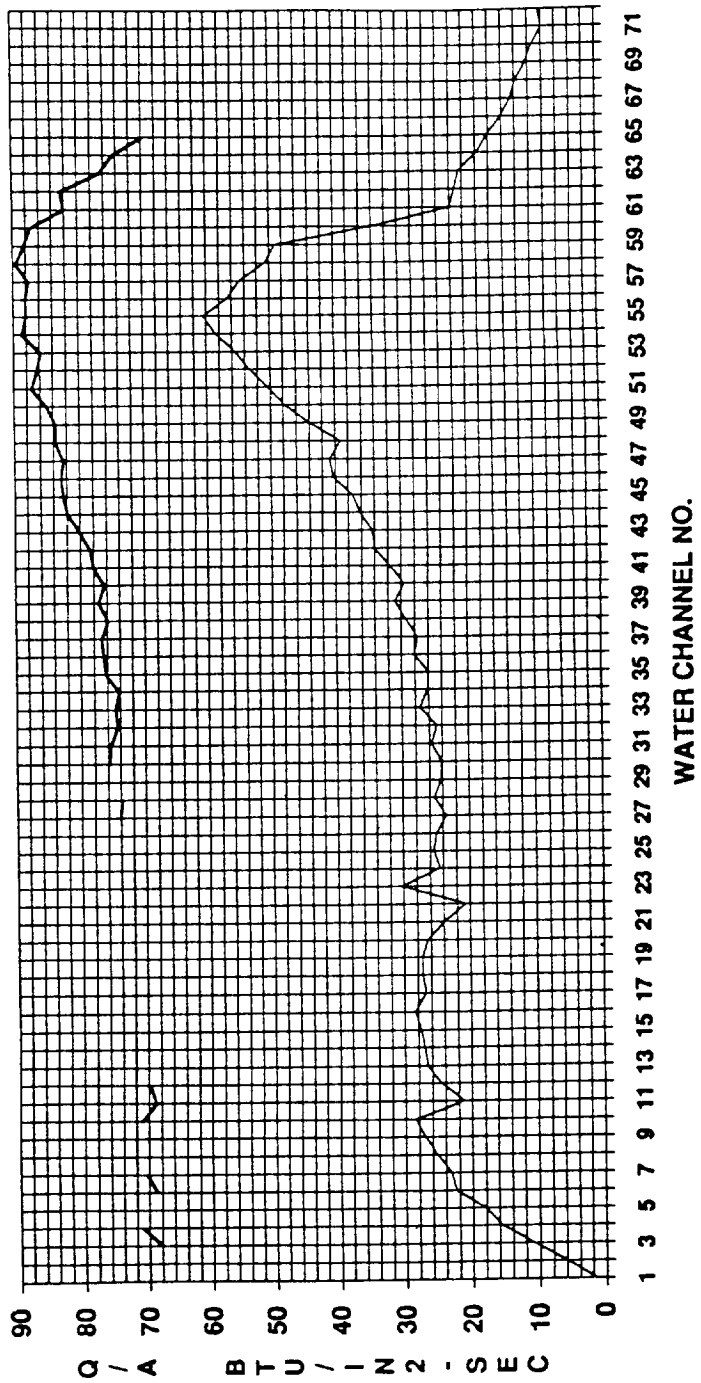

Appendix B: P&W Data

Ref 11

Subscale Nozzle Film Cooling Predictions

Empirical Correlation, TDK and CFD Heat Flux Comparisons

"ALLOWABLE" HEAT FLUXES

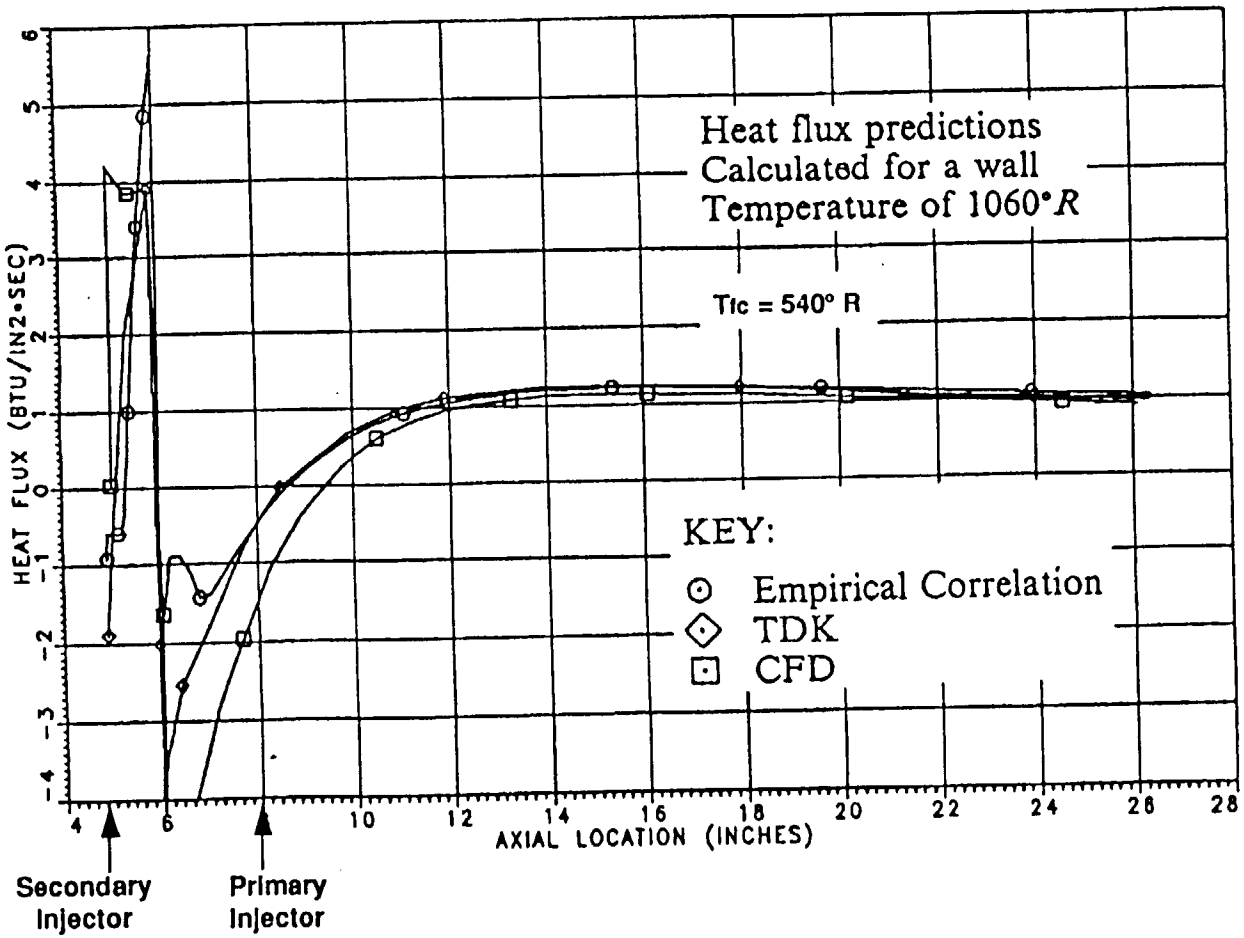

58

PW-MCC-0691-OAR-01PP-38